Mathematics

AIMS Mathematics, 10(6): 14392–14433.
DOI: 10.3934/math.2025648
Received: 17 April 2025
Revised: 21 May 2025
Accepted: 28 May 2025
Published: 23 June 2025

https://www.aimspress.com/journal/Math

Research article

Sequential topology optimization and reliability analysis using bisection: Level-set vs MIST, SIMP and ESO methods with multi-source uncertainties

Yiqing Shi[1], Mahmoud Alfouneh[2,*] and Chao Yuan[1,3,*]

[1] China Academy of Machinery, Beijing Research Institute of Mechanical & Electrical Technology Co., Ltd., Beijing, 100083, China
[2] Affiliation Department of Mechanical Engineering, University of Zabol, Zabol, P.B. 9861335856, Iran
[3] School of Mechanical Science and Engineering, Huazhong University of Science and Technology, Wuhan, 430074, China

* **Correspondence:** Email: alfoone@uoz.ac.ir, yc13718047495@163.com.

Abstract: The deterministic topology optimization (TO) has become one of the better-known optimization approaches in the engineering design of structures. However, its approximation errors have placed several restrictions on designers as it does not consider inherent uncertainties such as loads, geometrical dimensions, and materials in structures. To remedy this issue, the TO methods were incorporated with reliable design with highly martials involved under uncertainties for structural/mechanical problems. In the current reliability-based topology optimization (RBTO) procedures under multi-source uncertainties, dynamic mean value (DMV) was applied for evaluating the probabilistic constraints. For this aim, a sequential TO and reliability analysis (STORA) was proposed for application in various TO methods. The TO loop coupled bisection method as inverse topology layout applied in reliability loop that the DMV was utilized for evaluating the probabilistic constraint using sufficient descent condition. In the current RBTO model based on STORA, different TO methods named moving iso-surface threshold (MIST), evolutionary structural optimization (ESO), Level-set, and solid isotropic material with penalization (SIMP) are discussed for various problems with continuous design domains. The comparative results are discussed for different TO methods basis bisection approach for TO and RBTO solutions. The results demonstrated that the stable results provided by DMV and different optimal shapes between inverse TO-based bisection and RBTO

solutions are captured. The proposed RBTO method using STORA provides safe optimum shapes for almost TO methods with uncertainties in material properties and loads.

Keywords: reliability-based topology optimization; level set; dynamic mean value; SIMP; MIST
Mathematics Subject Classification: 54A10

1. Introduction

The main purpose of topology optimization (TO) is to a distribute given materials optimally inside a fixed design domain to address an objective function according to specified response of the structure. The extensive studies found how the field of TO can be attractive, challenging, and useful [1]. The comprehensive literature and textbooks are applied to find various methodologies of TO [2–5]. In TO approaches, it is usually conducted in an explicit methodology by ignoring the natural uncertainties in loads, manufacturing tolerances, geometrical dimensions, and materials of the structures [6]. Conversely, to rectify such a manner and encompass the effects of uncertainties in the optimal design layouts of the structure with the aid of probabilistic constraints conception, consequently, reliability-based topology optimization (RBTO) has been applied as a useful tool to evaluate the uncertainties in probabilistic constants of TO methods.

Topology optimization under multi-source uncertainties can be applied to design engineering structures effectively for obtaining safe optimal conditions [7,8]. Kang and Luo [9] evaluated the uncertainties in the structure, which take nonlinearities with the multi-ellipsoid convex model. Non-probabilistic reliability-based topology optimization (NRBTO) was applied in [10,11] for the multi-layer composite structures under anisotropic constitutive relationship [10]. NRBTO, with stress constraints, was also applied in the study of Xia and Qiu [11] with the aid of a sequential strategy where a shift function was utilized to circumvent the numerical instabilities during the optimization course [9,11]. It was observed through numerical examples that it is feasible to obtain optimal structures under stress-based NRBTO procedures. In the work of Zhang and Ouyang [12], the level set method was applied as a topology optimization scheme where the uncertainties were loads and geometric dimensions for designing coherent mechanisms. For RBTO, a sensitivity technique using gradient optimization has been proposed for TO-based level set strategy, and failure probability is estimated using Monte Carlo simulation for life cycle of continuous structures [13]. A RBTO using a two-phase approach has been established for continuum structures where, in the first phase, the deterministic TO is performed, and the RBTO model is used in the second phase for considering compliance TO problems [14]. The RBTO results of multi-material structures with interval loading uncertainty are investigated based on a robust TO model for linear elastic compliance structures where uncertainty in loads is decomposed into a two-unit force [15]. RBTO was applied for three-dimensional (3D) optimization by means of an extension of smoothing evolutionary structural optimization (SESO) and sequential element rejection and admission (SERA) [16]. The performance index approach and a filtering scheme adopted especially for solid isotropic material with penalization (SIMP) were presented in the presence of maximum displacement as a constraint. It can be given from the literature that the TO methods for computing optimal layouts and the reliability analysis approaches for evaluating the probabilistic constraints are two major challenges in RBTO methods. The TO methods and reliability approaches can affect the optimal shape configuration of

continuous structural problems [17]. The different TO methods applied for determining the shape layouts may provide different configurations with probabilistic constraint. The comparative TO methods applied in RBTO can be investigated for optimal shape layouts of continuous structural TO problems under load and martial uncertainties. Moreover, the combination of TO with probabilistic limitations is extremely demanding and challenging, that is, numerically complex and inconvenient for straightforward approximation to the failure probability. Thus, there is a gap for investigating the different TO methods incorporating probabilistic constraints. On the other hand, the different topology optimization methods may provide different shape layouts of optimum configurations for continuous structures by changing their formulations and methodology. Further, it has been shown that the numerical ability robustness of the analytical reliability method applied in RBTO can directly produce the stable optimum layouts under uncertainties [18]. Thus, a general method of RBTO is a main challenge for developing the various TO methods coupled by reliability approaches.

Such challenges and attractions of TO accounting uncertainties have encouraged the expansion and development of numerous uncertainty propagation approaches, such as the Monte-Carlo simulation (MCS) scheme [5,19,20] and the first and second-order reliability methods (FORM/SORM) [21–23]. Due to numerous obstacles around the MCS method, such as the requirement for large amounts of sampling data and repeating the analysis for each data set, two methods based on the FORM resolution, called the reliability index approach (RIA) [25–26] and performance measure approach (PMA) [28], were developed. Luo et al. [29] presented an effective approach for RBTO of a structure based on the PMA method. The RBTO and quantile-based TO were investigated by Zhang et al. [30], where the RBTO model is transformed into a quantile-based formulation in RBTO. The design optimization with interval uncertainty has been investigated using the possibility theory, where interval optimization is transformed into a series analyses named the double-loop nested optimization [31]. The PMA was adopted by Cho et al. [32] to assess the probabilistic constraints that were applied in the electro-thermal-compliant mechanisms to derive optimal topologies. In compliance with the extensive studies in which PMA and RIA methods were implemented, it was shown that PMA is better than RIA because of its better convergence and efficiency [33–35]. Moreover, methods such as PMA and RIA, which are FORM analytical methods, are based on double-loop approaches with high computational costs and low convergence, and methods such as the single-loop method, sequential TO, and reliability methods basis PMA are recommended [36–38]. One of the methods used for decoupling the RBTO solution is sequential optimization and reliability assessment (SORA) [39–41]. In SORA, the transformation of probabilistic constraints takes place into explicit constraints by moving the boundaries of defined constraints to the achievable path established on the reliability information extracted in the previous iteration. Cho and Lee. [42] investigated the use of an enhanced SORA created by convex linearization utilizing the sensitivity and function value of the probabilistic constraint at the most probable point (MPP) in which reliability and deterministic analyses were performed sequentially. In this work, for both efficiency and accuracy, the RBTO-based SORA are considered for evaluating optimal shape layout under multi-source uncertainties.

The instabilities of FORM with a chaotic solution in reliability methods without control schemes such as Armijo [43] or sufficient descent [44] rules are shown when probabilistic constraint is approximated with nonlinear relations [18,45]. By increasing nonlinearity degree in probabilistic constraints, it may provide unstable solutions as periodically and chaotic results for iterative formulas of analytical reliability methods and FORM [46–49]. Since there are instabilities for chaotic and periodic iterations of FORM, Keshtegar [46] proposed the nonlinear discrete chaotic conjugate map

using a chaotic step size that was regulated, relying on a finite-step size utilizing Armijo line search and logistic map to seek MPP. In the study of Keshtegar and Alfouneh [18], accelerated FORM was used to determine MPP. The machine learning scheme derived from the support vector regression (SVR) was implemented to estimate the probabilistic constraint to enhance computational expenses. Moreover, the moving iso-surface threshold (MIST) and dynamical accelerated mean value were used as a performance measure approach in RBTO [50–52]. This showed that the FORM method formulated by a sufficient decent condition [53] can be applied to search MPP for probabilistic constraints to consider the multi-source uncertainties in RBTO-based sequential topology optimization and reliability analysis (STORA). The dynamic step factor played an important role in the integration of TO and reliability iterative methods. Nevertheless, a general framework should be extended for RBTO that can be applied in different TO methods. As given from research, the advantages of various TO methods for robustness, accuracy, and computational burden are the vital challenges for computing optimal volume fraction as the inverse method in RBTO. The STORA have been investigated by applying different TO methods for optimum configurations of continued structural problems that some of these TO methods call a level set [54], MIST, SIMP, and evolutionary structural optimization (ESO) [55]. Performing RBTO, the reliability and TO methods are two major frameworks in STORA for stable reliability results as MPP search and accurate volume fraction as optimum shape layouts for achieving a safe design with multi-source uncertainties [56]. Consequently, robust formulation of the iterative reliability method applied in the reliability loop can provide a stable MPP for different TO methods under multi-source uncertainties. However, the optimum layout configuration of structures under uncertainties may be remarkably dependent on the TO methods. On the other hand, investigations of various TO methods in RBTO solutions are the other efforts in this work.

In this investigation, the STORA method for RBTO solution is proposed as the novel RBTO solution for comparing the different TO methods. Initially, in the inverse TO solution (TO integrating bisection method with an allowable probabilistic constraint) with a prescribed allowable probabilistic constraint in conjunction with the bisection method and considering one of the TO methods, optimal volume fraction and thereby optimal layout are derived. In the RBTO step, normal TO optimization is performed with the mean volume fraction and the element-based densities/results are employed for reliability methods derived by a dynamical mean value method extracted based on a sufficient and decent condition. This flowchart is repeated for every proposed TO method, and results are compared collectively. The results show that for every TO approach, the RBTO solution delivers a structure with more reliability and safety than an inverse TO procedure with completely different optimal configuration.

2. The TO with different approaches

RBTO solution includes an inverse TO solution where the TO solution is conducted by the following TO model:

$$\begin{gathered} min/max: \Gamma(\rho), \\ \text{Subject to: } G_i(\rho) \geq 0 (i = 1, \dots, m), \\ \sum_{e=1}^{nel} \rho_e v_e - V_f \sum_{e=1}^{nel} v_e \leq 0, \end{gathered} \tag{1}$$

$$0 < \gamma \leq \rho_e \leq 1,$$

where ρ is the vector of independent deterministic design variables (i.e., the element densities). $\Gamma(\rho)$ is the objective function which is structural compliance in this study. $Gi, (i = 1,2, \ldots, m)$ is the i-th limit state function or performance function. V_f is the mean or optimum volume fraction obtained by the inverse TO or RBTO based bisection method, which will be introduced in sections 4 and 5 or the initially given volume fraction $\frac{V_f}{V_{f0}}$ (mean value). v_e is the volume or area of the element. ρ_e is the density or weighting factor of e-th element (e =1,2, 3, …, nel). γ is the value chosen for impeding of the singularity of stiffness matrix with the lowest value 10^{-3}.

Different TO approaches are presented, and the statement for optimization problem by each TO method is described below:

2.1. Solid isotropic material with penalization

The SIMP [57] is a density-based TO method in which, for each element, a density or weighting factor ρ_e that varies between a low value γ and maximum value 1 is assigned, meaning there are intermediate elements in the design domain. Because the relative density of the material can steadily alter, the elasticity modulus of material for each element can also change. For each element, the formulation that relates the density of element to the elasticity modulus can be written as follows:

$$E = E_{min} + \rho^{\bar{P}}(E_0 - E_{min}). \tag{2}$$

The penalization factor $\bar{P}$ diminishes the involvement of elements with intermediate densities called grey elements. It pushes the optimization process in the direction that elements with $\rho_e = 1$ (solid or black elements) and elements with $\rho_e = \gamma$ (white or void elements) remain in the design field. $\frac{E_{min}}{E_0} = 10^{-9}$ is chosen to avoid singularity in the stiffness matrix. E_0 (mean elasticity modulus) refers to the Young's modulus of a solid element. The optimization problem intending to find a solution for the minimum compliance using the SIMP method can be given as follows:

$$\begin{gathered} min \quad \Gamma(\rho) = Y^T KY = \sum_{e=1}^{nel} \rho_e^{\bar{P}} y_e^T k_e y_e, \\ \text{subject to: KY} = \text{F}, \\ \sum_{e=1}^{nel} \rho_e v_e - V_f \sum_{e=1}^{nel} v_e \leq 0, \\ 0 < \gamma \leq \rho_e \leq 1, \end{gathered} \tag{3a}$$

where Y, K, and F are the global displacement vector, the global stiffness matrix, and the global load vector, respectively. V is the total area or volume of the design domain y_e and k_e are the elemental displacement vector and stiffness matrix, respectively.

An assembly of the elemental stiffness matrix can be seen in the following form:

$$K = \sum_{e=1}^{nel} \rho_e^{\bar{P}} k_e \text{ where } k_e = \int_{\Omega^e} B^T \tilde{D}\, B d\Omega. \tag{3b}$$

Here, B is the strain-displacement matrix and $\tilde{D}$ is the elasticity matrix.

Sensitivities of the objective function with regard to ρ_e can be computed as follows:

$$\frac{\partial \Gamma}{\partial \rho_e} = -\bar{p}(E_0 - E_{min})\rho_e^{\bar{p}-1} y_e^T k_e y_e. \tag{4}$$

After introduction of the SIMP method by Bendsoe and Kikuchi [1], it was developed in many ways with the collaboration of different methods, and some were coded as an open source code for 2D and 3D structures. Initially, Sigmond [58] published a MATLAB code for TO of 2D structures considering structural compliance minimization as the objective function. This code was extended to the 3D structures as 3D-SIMP by Liu and Tovar [59] in MATLAB codes. The TO solvers were sequential quadratic programming [60,60] and method of moving asymptotes [62,62]. Andreassen et al. [64] introduced a higher efficiency by pre-allocating arrays and vectorising loops.

The gradient projection-based method (GPM) was an efficient development of SIMP, which was applied for structural topological optimization compliance minimization indicated by a nonlinear objective function that is minimized over a possible design domain expressed by mutual borders and a single linear equality constraint [65]. This method utilizes the following approaches to enhance the effectiveness of the method by 1) using clipping and an adapted projection of searching direction, 2) introducing an analytical resolution proposed to evaluate the projection with the least computation and memory usages, and 3) shortening the searching step computation. The detail of this method can be found in [65]. A concurrent TO method of modified SIMP developed by Gao et al. [66] merges TO with an energy-based homogenization method to assess the macroscopic effectual properties of the microstructure for the composite structures.

2.2. ESO/ bi-directional evolutionary structural optimization

ESO [2,50] is a method of TO in which the elements that are weak and have less contribution to the structural analysis are removed systematically. Due to its simplicity and ease of programming, the method was used for complex problems [67–69]. In the case of stress in the structure, ESO uses criteria to remove inadequate elements. This criterion is defined as the respect of Von Mises stress level of each element σ_e^{vm} to the maximum Von Mises stress σ_{max}^{vm} of the whole structure in a finite element analysis (FEA) solution and can be shown as follows:

$$\frac{\sigma_e^{vm}}{\sigma_{max_i}^{vm}} < RR_i, \tag{5}$$

where RR_i is the current rejection ratio. The current RR_i is increased to the next iteration of optimization by an evolutionary rate (ER) when the current iteration reaches a steady state, and no extra elements are eliminated.

$$RR_{i+1} = RR_i + ER. \tag{6}$$

Due to sometimes encountering an ESO solution to the local optimal point and requiring initial oversized design domain, the bi-directional evolutionary structural optimization (BESO) was proposed to add or remove materials in the course of optimization to treat this issue based on the following criteria:

$$\begin{cases} \frac{\sigma_e^{vm}}{\sigma_{max}^{vm}} < RR_i \quad (element\ removal), \\ \frac{\sigma_e^{vm}}{\sigma_{max}^{vm}} > IR_i \quad (element\ addition), \end{cases} \tag{7}$$

where IR_i refers to the current addition ratio (IR). Due to some theoretical problems in TO [70], Rozvany and Querin [71] suggested that the void element should be substituted by a soft element, and a penalized scheme similar to the SIMP method according to Eq (2) must be imposed. Even though it was demonstrated that this solution gives better results than SIMP, the ESO/BESO was further developed to create smooth boundaries, by Liu et al. [72].

The TO problem with the ESO method is stated as follows:

$$\begin{gathered} min \quad \Gamma(\rho) = \frac{1}{2} Y^T K Y = \frac{1}{2} \sum_{e=1}^{nel} y_e^T k_e y_e, \\ \text{subject to: KY} = \text{F}, \\ \sum_{e=1}^{nel} \rho_e v_e - VV_f = 0, \\ \gamma \leq \rho_e \leq 1. \end{gathered} \tag{8}$$

The sensitivity S_e of each element is computed by the following equation:

$$S_e = \frac{\partial \Gamma}{\partial \rho_e} = \frac{1}{2} y_e^T k_e y_e. \tag{9}$$

The extended finite element method (XFEM)-ESO is an application of ESO that was introduced by Abdi [73]. This method integrates XFEM with ESO, which was previously limited to the level set (LS) methods. XFEM, as an alternative to the classical FEM method, was found to be thriving as a powerful tool in numerical analysis related to the TO. XFEM was introduced to demonstrate discontinuities, such as cracks and material-void interfaces, within the finite elements.

TriTOP is another application of the BESO method [74], which uses unstructured triangular mesh with the advantage of removing zig-zag boundaries emerging while applying a rectangular mesh. The important step in this method is solving the balance of a truss network to produce the body-fitted mesh. To make boundaries smoother and relive the structure complexity, the nonlinear diffusion approach was implemented. The BESO method was also applied in the study of Kazakis and Lagaros [75] where a multiscale TO was performed to compromise concurrent optimization of two separate scales: The macro-scale and the micro-scale. The macro-scale, which considers the overall size of the structure, consists of unit periodic micro cells that can represent a targeted part or the whole of structure.

2.3. Moving iso-surface threshold

MIST [76] is an improved TO approach that was developed recently. This method has been applied for several statics [77,77] and dynamic problems [79,80], and satisfactory results were derived. It uses the features of previous well know topology optimization methods such as i) applying the density-based scheme as in SIMP method, ii) utilizing the physical response function similar to ESO, and iii) establishing the progressing material boundary analogous to the level set methods in terms of the iso-value or iso-level [81]. Since this method employs Karush-Kuhn-Tucker conditions [82], it

does not require fulfilled direct sensitivity analysis. On the other hand, because of the simplicity of the method, it can be readily interfaced with popular FEM software such as ANSYS [83] and NASTRAN [84].

The key step in MIST is to seek a physical response function Θ that is integrated over the design field Ω to update and give the element densities or weighting factors an intersection of a physical response function, 3D surface with an iso-surface threshold t. The 3D surface of the physical response function is constructed over a 2D design domain in which z values are the nodal or Gauss point values of a physical response function. The iso-surface threshold t, which is computed by a sorting or bisection method (different from the one that is presented in Section 5) through normalized and filtered physical response functions cutting the 3D surface and giving the element densities. In that case, elements completely above the iso-surface threshold assign values equivalent to one, and the ones underneath the iso-surface threshold obtain element densities equal to γ. For the element that is cut by the iso-surface, its element density is the area or volume above the iso-surface to the total area of the element. A penalization scheme like the SIMP is also employed to penalize the elements that are not involved in the structural analysis and are weak. The global stiffness of the structure in that case can be written as follows:

$$K = \sum_{e=1}^{nel} \rho_e^{\bar{P}} k_e. \tag{10}$$

The topology optimization problem statement using the MIST can be given as follows:

$$min/max: \Gamma(\rho) = \int_{\Omega} \Theta(\rho)\, h(t,\Theta) d\Omega,$$

$$\text{S.t.} \begin{cases} KY_{(1)} = \dfrac{F_{(1)}}{min\,\Gamma(\rho)} & \text{Applying true load}, \\ KY_{(2)} = F_{(2)}, & \text{Applying virtual load}/\, max\,\Gamma(\rho), \\ \int_{\Omega} h(t,\Theta) d\Omega \le V_f V, & \\ 0 < \gamma \le \rho_e \le 1. & \end{cases} \tag{11}$$

Here

$$\Theta(\rho) = \frac{1}{2}\sigma_{(1)}\varepsilon_{(1)} \quad \text{true load/min}\Gamma(\rho),$$

$$\Theta(\rho) = \frac{1}{2}\sigma_{(2)}\varepsilon_{(1)} \quad \text{virtual load/min}\Gamma(\rho) \quad \text{and} \quad h(t,\Theta) = \begin{cases} 1\Theta \ge t, \\ 0\Theta < t, \end{cases} \tag{12}$$

σ and ε are vectors of stress and strain.

2.4. Level-set method

In the level set method [85], the target structural layouts are stated implicitly, employing the iso-surface by means of the level set scalar function. The optimal shape changes its feature during the optimization process with the updating of the level set function. Consider there is an implicit function $\phi(x,t)$with gradient $\nabla\phi$ in the design domain Ω with the smooth boundaries to satisfy the following conditions:

$$\begin{cases} \phi(x,t) > 0 & \forall x \in \Omega \backslash \partial\Omega, \\ \phi(x,t) = 0 & \forall x \in \partial\Omega, \\ \phi(x,t) < 0 & \forall x \in D \backslash \Omega, \end{cases} \tag{13}$$

where $x \in D \subset \{(x,y)|x,y \in \Re\}$ is every point in domain D, and $\partial\Omega$ is the solid boundary. D is a bigger domain that encloses Ω, and t is pseudo-time. The differentiation of the level function to t gives the following level set equation (Hamilton-Jacobi equation):

$$\frac{\partial\phi}{\partial t} + \tilde{V}_n|\nabla\phi| = 0, \tag{14}$$

where $\tilde{V}_n$ refers to the normal velocity of the interface in n direction and

$$\tilde{V}_n = \tilde{V} \cdot \frac{\nabla\phi}{|\nabla\phi|}. \tag{15}$$

The compliance optimization problem utilizing the level-set method can be expressed as follows [86]:

$$min: \Gamma(\phi) = \frac{1}{2}\int_\Omega E(\phi)\varepsilon(\tilde{u})^T \tilde{D}\varepsilon(\tilde{v})d\Omega,$$

$$\text{S.t.} \quad \int_\Omega E(\phi)\varepsilon(y)^T \tilde{D}\varepsilon(\tilde{v})d\Omega = \int_\Omega p \cdot \tilde{v}d\Omega + \int_S \tau \cdot \tilde{v}d\Omega, \tag{16}$$

$$\int_\Omega H(\phi)d\Omega \leq V_f,$$

where p is body force, $\tilde{v}$ is the virtual displacement, τ is the traction imposed on the boundary S, and E is the design variable given as:

$$(\phi) = E_0 H(\phi) + \big(1 - H(\phi)\big)E_{min}. \tag{17}$$

Here, E_{min} denotes the minimum elasticity modulus, and $H(\phi)$ describes the Heaviside function as:

$$H(\phi) = \begin{cases} 0 & \phi \leq 0, \\ 1 & \phi > 0. \end{cases} \tag{18}$$

The element sensitives can be derived by the following formulation:

$$S_e = \frac{\partial\Gamma}{\partial\Omega}\Big|_e = -y_e^T k_e y_e. \tag{19}$$

The Filter-Based method is a simple and fast version of the level set method introduced by Yaghmaei et al., [87] that can be applied for complex problems, implementing density filters to level set functions to smooth optimized layouts. This method uses a control strategy to minimize the total potential energy equivalent to minimize structural compliance. The optimization problem is outlined as follows:

$$inf_\omega \quad J^{(1)}(\omega) = \int_{\bar{\Gamma}_N} \bar{t}_i \tilde{u}_i d\bar{\Gamma} - \frac{1}{2}\int_\omega \tilde{u}_{i,j} C^0_{ijkl} \tilde{u}_{k,l} d\Omega^0, \tag{20}$$

$$\text{S.t.} \tilde{G} = \int_\omega d\Omega^0 - V_{max},$$

where $\omega \subset D$ is the solid domain, and $\bar{\Gamma}$ is the ω boundary that includes two distinct parts of the Neumann boundary $\bar{\Gamma}_N$ and Dirichlet boundary $\bar{\Gamma}_D$. $\bar{t}_i$ is the surface force subjected to Neumann boundary $\bar{\Gamma}_N$. The superscript (1) stands for the minimum total potential energy problem. $\tilde{u}$ is the displacement, and C^0_{ijkl} is the solid domain fourth-order stiffness tensor of material properties. The block diagram of the filter based level set optimization is given in Figure 1 [88]:

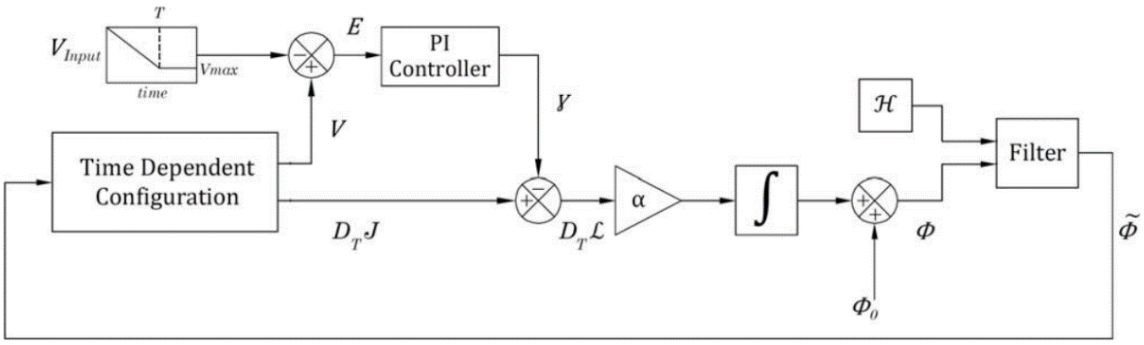

Figure 1. The block diagram for the filter based level set topology optimization method [86].

In TO, applying filtering plays a crucial role in sensitivity analysis by reducing localized fluctuations in design sensitivities, thereby addressing numerical issues such as checker boarding patterns and mesh dependence. This process enables more dependable and precise optimization outcomes while preserving the overall structural response within a design domain. In the SIMP method, the filtering scheme introduced by Sigmond [88] is implemented. ESO/BESO employs a similar sensitivity filtering scheme as SIMP. In this research, we impose regularization on the smoothness of the level set function by utilizing the filter proposed by Andreassen et al. [64]. In MIST, the $\Theta(\boldsymbol{\rho})$ function can be adjusted similarly to the method used in SIMP, where the $\Theta(\boldsymbol{\rho})$ values are altered based on a linear weighted average within a defined spatial neighborhood. Since the $\Theta(\boldsymbol{\rho})$ function values are determined at nodal positions, the center of the spatial filter for a particular node is at the nodal position, and the distances between neighboring nodes are calculated.

3. RBDO solution

The RBDO problem can be typically formulated as follows:

$$min: \Gamma(\rho),$$

$$\text{Subject to: } P_r[G_i(\rho, X) \leq 0] \leq \Phi\left(-\beta_t^i\right) (i = 1, \ldots, m),$$

$$\sum_{e=1}^{nel} \rho_e v_e - V_f \sum_{e=1}^{nel} v_e \leq 0, \tag{21}$$

$$0 < \gamma \leq \rho_e \leq 1,$$

where X denotes the vector of random variables (i.e., loads, geometrical dimensions, boundary conditions, and material properties). β_t^i is the target reliability index of the i-th performance function $G_i(\rho, X)$. P_r is the failure probability and Φ is the standard normal cumulative distribution function.

The RBTO solution using STORA consists of two major parts as solvers, including 1) TO for optimization solver and 2) reliability analysis for evaluating probabilistic constraints using MPP search methods. The MPP solution is applied for moving probabilistic constraints into safe design domains by using an analytical FORM method. The reliability part used in this study is an effective and enhanced method that is formulated based on the sufficient descent condition. The advanced mean value (AMV) approach is enhanced by utilizing a dynamical formulation that is developed using sufficient descent conditions on a beta-circle hyper-sphere as an iterative formulation. The modified AMV method is briefly formulated below:

$$U_{k+1} = \beta_t \frac{n_k}{\|n_k\|}, \tag{22}$$

$$n_k = U_k + \lambda_k [f(u_k) - U_k], \tag{23}$$

$$f(u_k) = -\beta_t \frac{\nabla_u G(d,U_k)}{\|\nabla_u G(d,U_k)\|}, \tag{24}$$

where U_k are normal standard random variables and $\nabla_u G(d, U_k)$ is the gradient vector of probabilistic constraint $G(d, U_k)$ at point U_k. d is related to design variable vector. β_t is the target reliability index. λ_k is a dynamical step size computed as below:

$$\lambda_k = min[0.75\beta_t, c_1 \frac{\|f(u_k) - U_k\|}{\|U_k - U_{k-1}\|}]. \tag{25}$$

In addition, $\lambda_0 = 1$ and $\|D_0\| = \beta_t$.

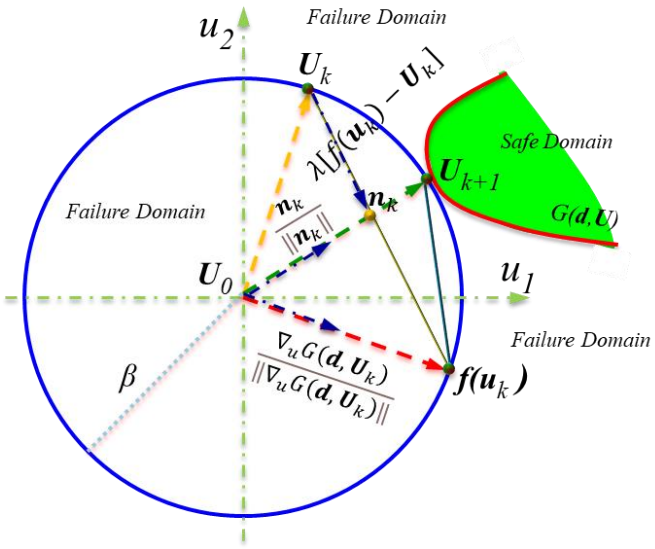

Figure 2. Schematic view of DMV for moving the probabilistic constraint from failure to safe domains.

The MPP is searched on a hyper-sphere with a radius of β_t. This iterative process using Eq (22), named the dynamical mean value (DMV) method, is applied for the MPP search because the step size in Eq (25) is dynamically adjusted at each iteration by using information of previous results. The DMV using formulation in Eqs (22–25) is schematically plotted in Figure 2. It can be given that the

probabilistic constraint is moved from the failure domain (mean point) to the safe domain (on the beta-circle). The searching point on the safe domain is the main effort of the reliability analysis that this point is related to the MPP. A dynamical controlling factor λ_k is used for giving the sufficient decent condition as $\|D_k\| \leq c_1\|D_{k-1}\|$.

In the DMV, the search direction is dynamically adjusted by a normalized vector $\boldsymbol{n}_k$ Eq (23), which is computed using λ_k. The computing process for step size using sufficient decent conditions is cited in Appendix A.

In this formulated FORM, the control factor is applied for giving a stable result by using the sufficient descent condition. The following steps are employed for searching the MPP in reliability analysis of RBTO which is given as below:

Step 1: Give $G(d, X)$ and β_t as the means of standard deviations and distributions of basic random variables.

Step 2: Set the stopping criterion (ε=10^{-4}), k=0, $\lambda_0 = 1$, $\lambda_{max} = 0.75\beta_t$, 0<c_1<1 i.e. $c_1 = 0.75$, and $X_0 = \mu_x$.

Step 3: Transfer variables from x-space into u-space as $u_k = \Phi^{-1}\{F_X(x_k)\}$ where $F_X(x_k)$ is the cumulative probability density function at point x_k.

Step 4: Compute $G(d, U_k)$ and $\nabla_u G(d, U_k)$.

Step 5: Determine $f(u_k) = -\beta_t \frac{\nabla_u G(d,U_k)}{\|\nabla_u G(d,U_k)\|}$.

Step 6: Compute $D_{k-1} = U_k - U_{k-1}$ and $D_k = f(u_k) - U_k$.

Step 7: Adjust $\lambda_k = min\{\lambda_{max}, \lambda\}$ where $\lambda = c_1 \frac{\|D_{k-1}\|}{\|D_k\|}$.

Step 8: Compute the new point as $U_{k+1} = \beta_t \frac{U_k + \lambda_k D_k}{\|U_k + \lambda_k D_k\|}$.

Step 9: If $\|U_{k+1} - U_k\|/\|U_k\| < \varepsilon$, then give MPP as X_k; Else $x = F_X^{-1}\{\Phi(u)\}$, set $k = k + 1$ and go to Step 3.

It can be given from the above steps that the iterative procedure using the DMV is established based on the control factor, which is simply computed by information given from the previous points.

4. Sequential TO and reliability analysis using the bisection method (inverse TO)

The bisection method is used to find the optimal volume fraction based on the given compliance U_c as the ultimate (allowable) probabilistic constraint and a range of volume fractions. This is actually an inverse TO optimization in relation to the TO formulation presented in Eq (1). The bisection is used for TO, and RBTO using MPP was originally represented in [14] and can be formulaically expressed in Eq (30) as:

$$\begin{aligned} &\text{Find} \quad V_f, \\ &min \quad \Gamma(\rho) = U_c, \\ &\text{S.t.} \quad G_i(\rho) \geq 0 (i = 1, \ldots, m), \\ &\sum_{e=1}^{nel} \rho_e v_e - V_f \sum_{e=1}^{nel} v_e \leq 0, \\ &0 < \gamma \leq \rho_e \leq 1. \end{aligned} \tag{26}$$

The TO-based bisection (inverse TO) is a framework of the TO, as presented in Figure 3, and is applied for the TO of a structure where the main constraint of the TO model is related to accepting the band as

U_c. As seen in Figure 3, a loop of TO is applied for evaluating the optimum results of a TO model that the optimum of TO is related to the constraint of the invers TO model. In the TO model, the main effort is the optimum as the minimum/maximum of $\Gamma(\rho)$ represented to comply in this study with the termination criteria where convergence is achieved when the difference between two consecutive design variables become less than a prescribed criteria value or a very low value.

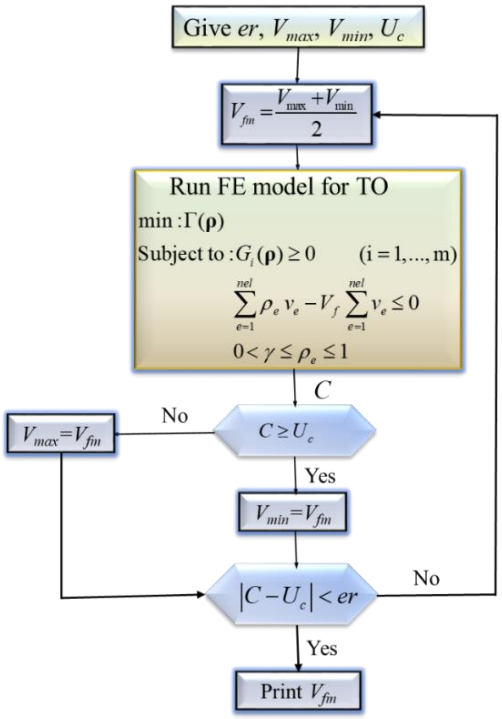

Figure 3. Framework of the inverse TO model using a bisection algorithm.

However, the $\Gamma(\rho)= U_c$ is the effort of the inverse TO model presented in this study, named TO-based bisection. To receive the optimum results of the TO method as $\Gamma(\rho)= U_c$, it updates the volume fraction by an iterative framework as see in Figure 3. As seen, the V_f is searched in interval V_{max} and V_{min} where the bisection framework coupled with TO is a free gradient-based method, and the optimum V_f is computed based on an iterative approach with robust results. It provides a framework for inverse TO-based different methods for finding the optimum V_f when $\Gamma(\rho)= U_c$. The V_f is adjusted based on related $\Gamma(\rho)$ until it is extracted as V_f, which provides $\Gamma(\rho)= U_c$ for compliance TO problems. The output of TO-based bisection is optimum V_f with $\Gamma(\rho)= U_c$ but the output of TO models is optimum with $\Gamma(\rho)$constant V_f. In the inverse TO model, we use the results of the TO model to update the V_f related to $\Gamma(\rho)= U_c$; thus, the capability and robustness of the TO methods are directly affected by the results of inverse TO methods.

The probabilistic constraint, by giving the multi-source uncertainties for $\Gamma(\rho)= U_c$, can be evaluated using the DMV reliability method to move the $\Gamma(\rho)$ in a safe domain, while in the TO-based bisection, the optimum V_f is the main effort with $\Gamma(\rho)= U_c$.

The proposed RBTO solution using the STORA approach is an integration of inverse TO given by different TO methods, and the reliability approach using DMV-MPP search. In the inverse TO method, the bisection approach is used to derive the optimal volume fraction when the optimum result of the TO model is equal to optimum constraint U_c. The reliability loop is applied for moving the

optimum constraint U_c in a safe domain. The result of STORA using a hybrid method of inverse TO and DMV is to find the optimum volume fraction with uncertainties in material and loads of structures. To receive the optimum V_f under uncertainties in STORA, two major frameworks as i) reliability-based DMV and ii) TO methods-based bisection are applied.

By having the MPP and the inverse TO method, optimized volume fraction and consequently optimal layout is derived for the RBTO problem. In that case, the RBTO problem using this procedure is given as follows:

$$\begin{gathered} \text{Find } d, \mu_x, \\ min \ \ f(\mathrm{d}), \\ \text{S.t.} \quad G_i(d, \mu_x - s_k^i) \geq 0 i = 1,2,\ldots,m, \\ \mathrm{d}^L \leq d \leq d^U, \mu_x^L \leq \mu_x \leq \mu_x^U, \end{gathered} \tag{27}$$

where s_k^i is the shift vector of i-th probabilistic constraint at k-th iteration, which is approximated as:

$$s_k^i = \mu_x - X_{k-1}^i, \tag{28}$$

and when Eq (27) integrates with the bisection method to derive the optimal V_f employing MPP extracted from DMV solution, the optimization problem can be formulated as follows:

$$\begin{gathered} \text{Find} \quad V_f, \\ min \quad \Gamma(\rho) = U_c, \\ \text{S.t.} \quad G_j(\rho, s_k^i) \geq 0 (i = 1,\ldots,m), \\ \sum_{e=1}^{ne} \rho_e v_e - V_f \sum_{e=1}^{ne} v_e \leq 0, \\ 0 < \gamma \leq \rho_e \leq 1, \end{gathered} \tag{29}$$

where $G_i(\rho, s_k^i)$ is i-th probabilistic constraint with V_f and density vector of design elements (ρ). Figure 4 depicts the RBTO solution flowchart. As seen in this Figure, the TO loop approximates the optimum feature of design domain by determining the constraints as $G_i(\rho, s_k)$. The bisection method is utilized for determining optimum $\Gamma(\rho)$, which corresponds to allowable constraint (U_c), where V_f related to U_c is approximated utilizing the bisection scheme, and the optimum layout with V_f associated to U_c is also computed. The optimum results of TO are transmitted in reliability analysis for calculating the MPP. The MPP obtained from the reliability analysis loop is transferred to the TO loop for the new approximating optimum V_f. Loops are consecutively utilized for determining minimum feature structures issues utilizing uncertainties in material properties, sizes, and loads. The termination criterion for the RBTO and MPP is shown in Figure 4.

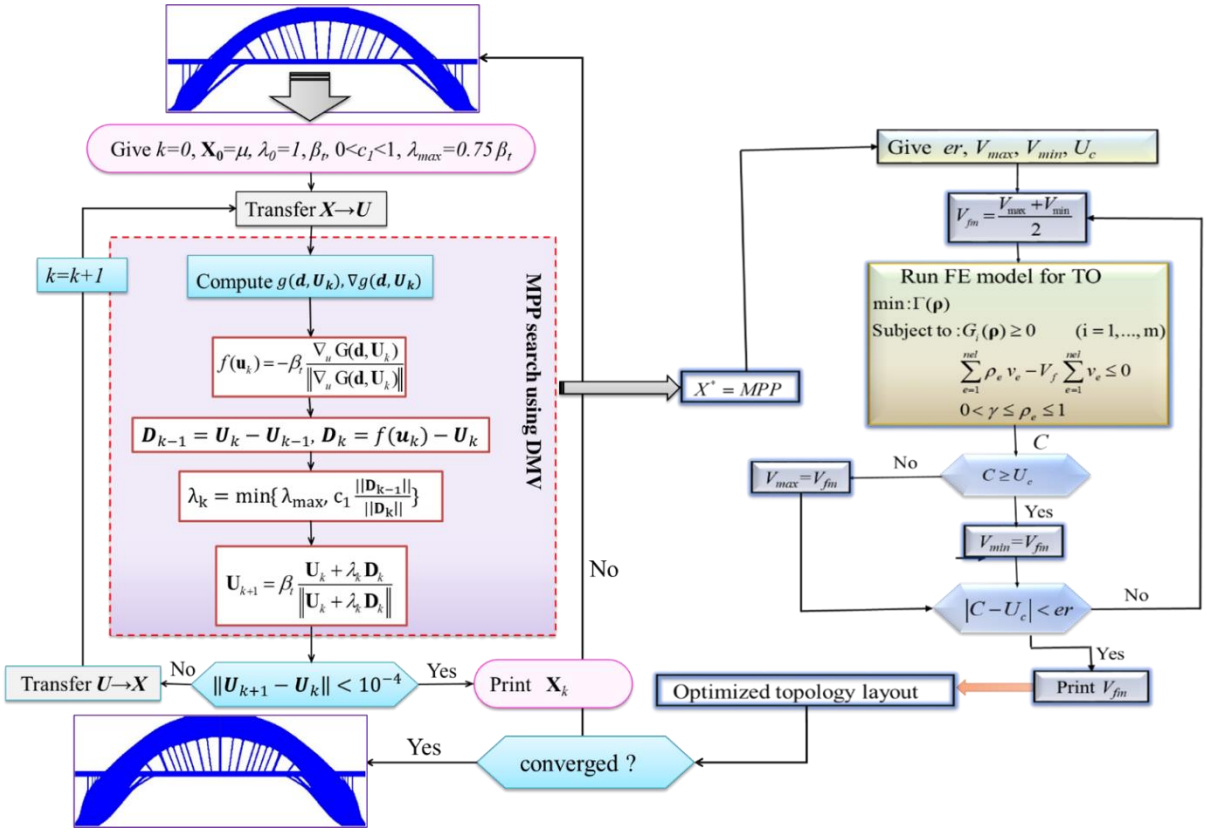

Figure 4. Flowchart for STORA using coupled inverse TO-based bisection and DMV for MPP search.

5. Numerical validation and applicable results

The proposed RBTO using STORA for different TO methodologies is applied to acquire a structure subjected to static loads. Topology optimization is performed for a variety of structures in different examples, and the results of proposed TO-based bisection and DMV for STORA are compared to confirm the robustness and capability of RBTO. Several TO methods are coupled in the inverse TO model for comparing the inverse TO and RBTO solutions. In all the examples, the TO in the results stands for the inverse TO.

5.1. Level-set method

For validation of the DMV method, two nonlinear mathematical cases are given for illustrating the abilities of four inverse FORMs named DMV, AMV, hybrid mean value (HMV) [89], and self-adaptive mean value (SMV) with parameters of C=0.95 and P=1.25 [90] with stopping criterion ε=10^{-4}.

Case 1: $g = exp(1.5x_1^{1.5} - 5) + exp(1.2x_2^2 - 15) - 15$ with normal variables of $x_1, x_2 \sim N(5, 0.8)$ and $\beta_t = 3.0$.

Case 2: $g = 0.3x_1^2x_2 - x_2 + 0.8x_1 + 1$ with normal variables of $x_1 \sim N(0,0.55)$, $x_2 \sim N(6,0.55)$ and $\beta_t = 3.0$.

The MPP search results using different reliability methods are presented in Figure 5 for cases 1 and 2. It can be concluded that the AMV and HMV produce unstable 2-priodic points while the SMV

and proposed DMV are robustly converged with similar iterations. The convergence line pattern of cases 1 and 2 using DMV are not similar to SMV because it depends on the step size with a dynamical adjusting process.

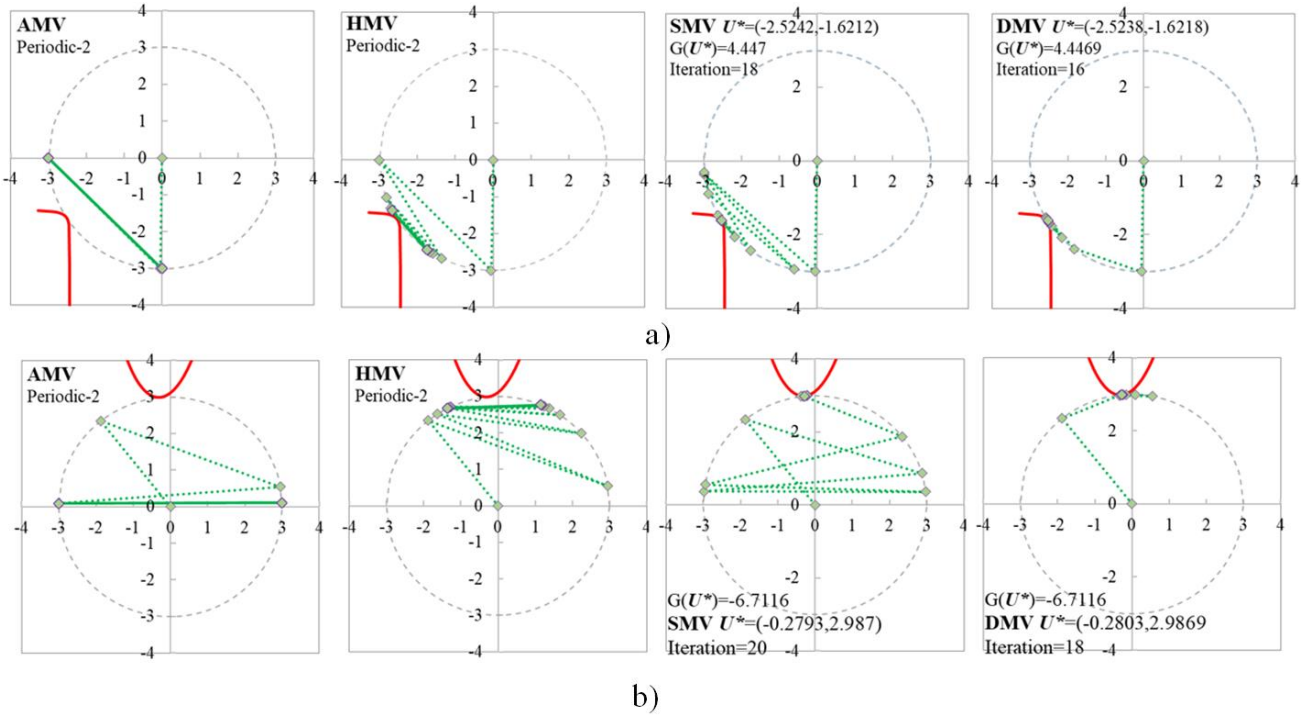

Figure 5. The convergence for MPP search using different reliability methods a) case 1 and b) case 2.

The step size is controlled based on the maximum value given as λ_{max}=0.75β_t that it is presented in Figure 6 for cases 1 and 2, which varies between zero and λ_{max}. As seen from Figure 6, the adjusting process with dynamical computation is demonstrated with iterations less than 20 more efficiently.

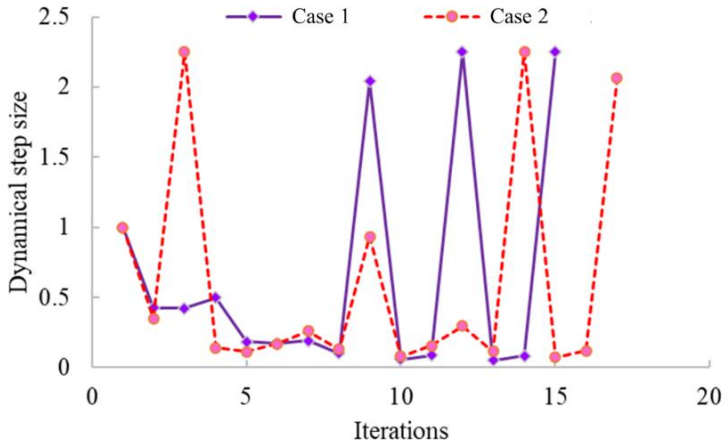

Figure 6. Dynamical step size obtained by the DMV method for cases 1 and 2 using λ_{max}=0.75β_t.

The robustness of the MPP search is obtained using the DMV formulation. The dynamical step size is dependent on two parameters of c_1 and λ_{max}. Different λ_{max} = (0.5,0.75,1.25,1.5) β_t with three conditions of sufficient descent by factor c_1 =0.75, 0.85, and 0.95 are compared with respect to iterations as computational burden efforts in Table 1 for Examples in cases 1 and 2. The results presented in Table 1 illustrated that the two major parameters as c_1 and λ_{max} factors remarkably affect the efficiency of reliability problems. By increasing factor c_1, the iterations are increased but the parameters of step size can be given as λ_{max} =0.75β_t and c_1 =0.75.

Table 1. Total iterations of DMV in different c_1 and λ_{max} parameters applied in cases 1 and 2.

λ_{max}	MAE (%)			RMSE		
	c_1=0.75	c_1=0.85	c_1=0.95	c_1=0.75	c_1=0.85	c_1=0.95
0.5 β_t	20	28	23	19	22	28
0.75 β_t	15	28	25	17	26	35
1.25 β_t	19	29	27	20	28	35
1.5 β_t	19	29	28	20	25	35

5.1.1. BBTO Example 1 for validation of TO

The procedure outlined in this paper is corroborated by the approach described in [91]. Specifically, Example 1 is examined by utilizing identical material properties, geometric dimensions, and boundary conditions, as illustrated in Figure 7.

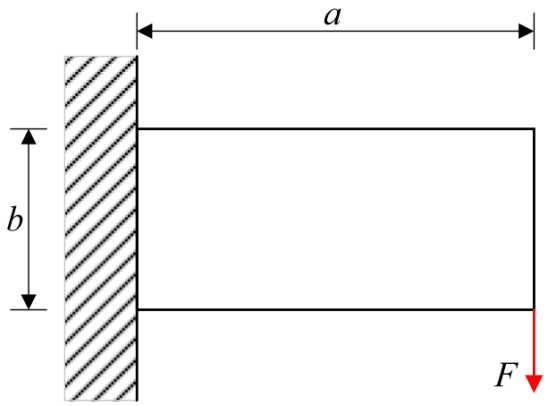

Figure 7. Design domain and boundary condition of a cantilever beam (a=150, b=100).

The design domain is discretised with 1500 SHELL181 ANSYS elements. Γ=U_c=2.4mm and β_t=3. Using the MIST method, $rmin$=3.5mm is the filtering radius and dynamic move limit is the move limit scheme. The random variables consist of elasticity modulus of E =200GPa and a load of F=20kN, each exhibiting a coefficient of variation (COV) of 0.1. The objective function Γ=2.4mm is the deflection of point under loading corresponding to the strain energy density at this point.

Utilizing the DMV methodology, the MPP values are recorded as 149.68GPa and 23.268kN. The optimized volume fraction for the RBTO solution, based on the calculated MPP values, has been established at V_f = 0.3481, which shows a minor discrepancy when compared to the value obtained from literature [91] as V_f =0.34653, which is given by the non-probabilistic reliability index for evaluating probabilistic constraint with the single loop optimization process. The methodology was

similarly employed with respect to the inverse TO, and the optimized volume fraction for the TO solution was determined to be V_f =0.1932, similar to V_f = 0.18844, which closely aligns with the value provided in [91].

Figure 8 illustrates the changes in the objective function throughout the optimization process for TO and RBTO solutions. This depiction emphasizes a consistent and convergent optimization path, reaching a final value of U_c=2.4mm to meet the probabilistic constraint. The TO solution initially demonstrates elevated values, indicating that a larger number of iterations is necessary for achieving convergence in the TO methodology.

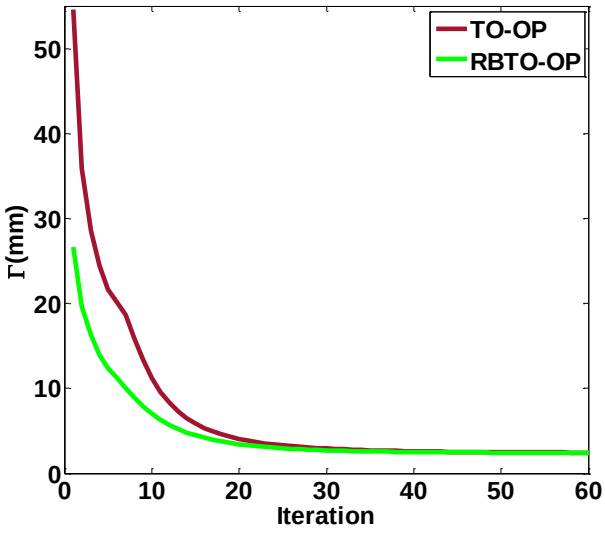

Figure 8. The objective function during the optimization process for TO and RBTO solutions.

The optimal configuration associated with the RBTO solution is depicted in Figure 9a, which closely resembles the figure available in the literature. Conversely, the optimal configuration for the TO solution is shown in Figure 9b, highlighting a design that employs considerably less material in TO by deterministic analysis without uncertainties in material and load. This indicates that the V_f increases when this problem involves uncertainties to move probabilistic in a safe domain. Consequently, the RBTO-based STORA given by the bisection method can provide an accurate result for evaluating RBTO problems.

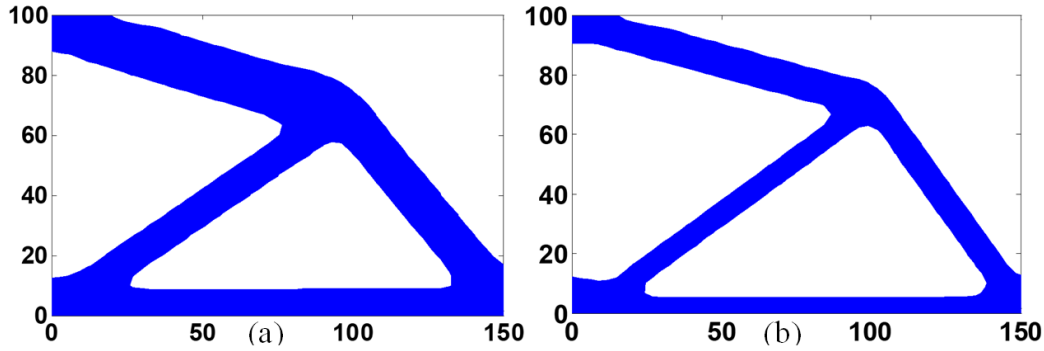

Figure 9. The optimal shape related to a) RBTO solution and b) TO solution.

5.1.2. Example 2-Design a gripper for evaluating the reliability method

The optimal design of the gripper is performed through the compliant mechanism design. The design domain is seen in Figure 10 in order to maximize the output displacement at the output point B where a true force P is applied at the input location A. To use the compliance mechanism design, a virtual unit load is applied at the output point B at the desired direction. Springs are placed in points A and B. The mean values of random variables are: $[k_1, k_2, E, P]$ = [0.1, 0.1, 1, 1]. The standard deviations for springs, E and P, are [0.05, 0.05, 0.01 and 0.1], respectively. Two methods of optimization, i.e. MIST and level set, are implemented to extract the gripper feature from the given design domain. In the MIST method, the design domain is discretised by 1710 PLANE182 ANSYS elements for plate and 2 COMBIN14 ANSYS elements for springs. In the level set method, 16200 quadrilateral elements are used. The initial values for each method are given as follows:

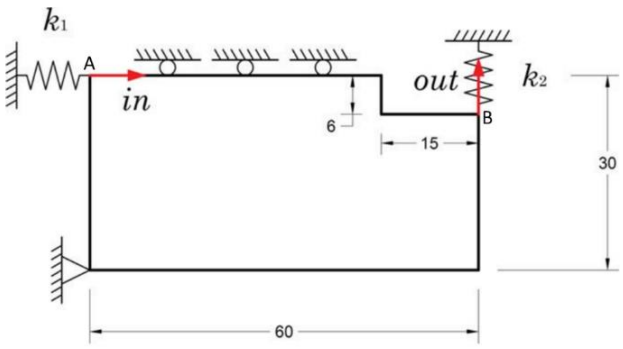

Figure 10. Working domain and boundary conditions for a gripper compliant validation Example 2.

where the input load is applied in point A and virtual unit load is applied vertically in point B.

I. MIST method: $penal$=3, $rmin$=3.

II. Level set method: PI= [5, 5], I_E=0, dt= 0.1, T=6, $Tinf$ =40, $penal$=10, and $rmin$=5 [87]. PI is proportional gain/integral gain, I_E is initial value for integral part, dt is factious time step, T is the time at which volume fraction is expected to reach V_{max}, and $Tinf$ is the total time for optimization process, with the number of time steps being $Tinf/dt$.

Eq (30) is used to depict the optimization problem along with the TO and RBTO solutions amid uncertainties.

$$\text{Find} \quad V_f^*, X^*,$$

$$\min \quad f(d) = \mathrm{V}_f,$$

$$\text{S.t.} \quad \Theta(\rho) = \frac{1}{2}\sigma_{(2)}^{T}\varepsilon_{(1),}$$

$$Y_{out}(V_f, \bar{k}_1, \bar{k}_2, E, P1) \geq 0.533,$$

$$0.1 \leq \mathrm{V}_f \leq 0.4, V_f = 0.2; \beta_t = 3,$$

where

$$\bar{k}_1, \bar{k}_2 \sim N(0.1, 0.05^2), E, P \sim N(1, 0.1^2), \tag{30}$$

$$\int_{\Omega} H(t, \Theta) d\Omega \leq V_f \leq \sum_{e=1}^{ne} \rho_e V_e,$$

$$(\rho_e^L \leq \rho_e \leq \rho_e^U), \Theta(\rho) = \frac{1}{2}\sigma_{(2)}^T \varepsilon_{(1)}.$$

The RBTO solution and to the inverse TO are applied, and the MPP values for uncertainties for both TO methods are: $[k_1, k_2, E, P]$ = [0.0944, 0.0944, 0.728, 0.575]. Based on MPP values, the optimum volume fraction for RBTO solution for the MIST method is V_f=0.28 in comparison to V_f =0.15 for TO. V_f for the RBTO solution for the level set method is 0.35, which is a bit larger than MIST and considerably larger than V_f =0.13 for its relevant TO. The results again highlight the benefits of incorporating MPP values in the optimal design of structures, considering variations in uncertainties to achieve a high-volume fraction compared to TO.

Figure 11 depicts the optimal TO and RBTO configurations for both MIST and level set approaches. It is evident that the best configurations using the level set method incorporate a greater number of ribs, leading to a design that is more robust and secure compared to the MIST approach. In general, the volume of material utilized in the RBTO solution is significantly greater than in the TO solution for both TO methods using the level set and MIST, indicating that the RBTO by considering the uncertainties with acceptable failure probability in the safe domain increases V_f about 45% for MIST and 60% for the level set method.

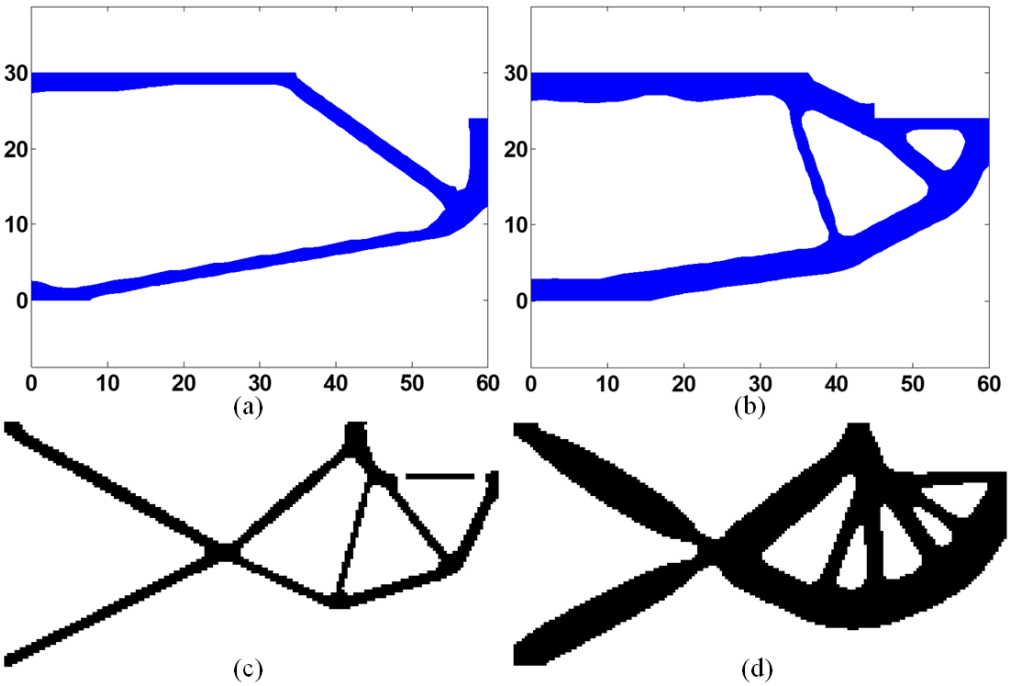

Figure 11. The optimal layout for TO and RBTO solutions for the gripper problem. a) TO for the MIST method, b) RBTO for the MIST method, c) TO for the level set method, and d) RBTO for level set method.

The iterations for convergence of reliability methods, i.e. DMV, SMV, AMV, and HMV for the structure in Figure 11d given from RBTO using the level set, are compared in Figure 12. As seen from these results, the AMV method does not capture stable results iterated as 2-priodic solution. However, the improved version of AMV formulated by DMV, HMV, and SMV are converged. The computational burden for achieving stable results is different by an improved version of AMV. The DMV is more efficient than the other methods, while the efficiency of SMV is better than HMV. This method can be applied for continues probabilistic constraint.

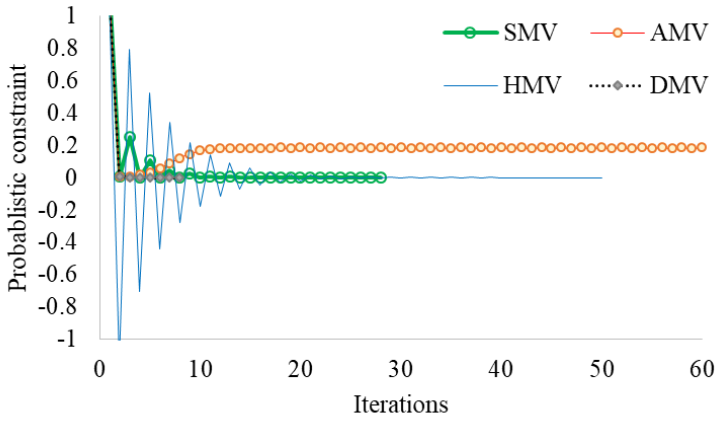

Figure 12. Iteration histories of probabilistic constraint for the gripper problem using different reliability methods with the RBTO layout structure obtained by the level set.

5.2. Comparative RBTO results

5.2.1. Example 3-the messerschmitt-bölkow-blohm structure

The messerschmitt-bölkow-blohm (MBB) structure is presented to investigate the inverse TO and RBTO solutions of the STORA approach subjected to the uncertainties of applying load (P_1) and material (E). The geometrical dimensions, boundary conditions, and loads are displayed in Figure 13. To conduct the FEA analysis, the structure is meshed with 2000 (100×20) same-size quadrilateral plane strain elements. The structure is mounted on a simply support on the lower, left corner and a roller support on the lower, right. The load is applied at the middle of the top edge. The Poisson's ratio υ =0.3 for all the examples is applied. For each of the TO approaches, the relevant initial pre-required data are given as follows:

Methods initial data:

I. SIMP method: Filter radius, $rmin$ =2, and $penal$=3 [58]. $rmin$ and $penal$ refer to filtering radius and penalty factor.
II. ESO method: vfi =1, er =0.01, MLP =0.99smax [73]. In ESO, vfi is the target volume fraction of the current iteration, er is the evolution rate, and MLP is the minimum level of performance.
III. MIST method: $rmin$=3, $penal$= 3, dynamic move limit [91].
IV. Level set method: r (radius of initial holes)= 0.1 $nely$, $cRBF$ (radial basis function parameter)=10^{-4}, $nLoop$ (the maximum iteration number of optimization) = 200, $nRelax$ (the volume constraint would be relaxed at first and then slowly tightened during

$nRelax$iterations)= 30, dt(the time step size) = 0.5, $delta$ = 10, mu (parameter in the k-th iteration)= 20, and $gamma$ (parameter in the k-th iteration) = 0.05 [85]. The initial guesses or initial designs are chosen by r and are selected as a signed distance function with only one initial hole in the center of the design domain where values are also limited between −3 and 3.

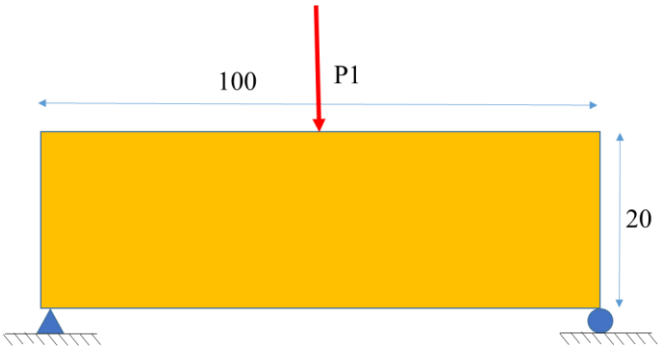

Figure 13. MBB beam with a force inserted in the middle of the top edge.

For this example, Eq (31) is presented to find the optimal shape for the RBTO solution:

$$\begin{gathered} \text{Find} \quad V_f, \\ \min \quad f(\mathrm{d}) = V_f, \\ \text{S.t.} \quad \mathrm{K}(\rho)\mathrm{Y}(\rho) = \mathrm{F}(\rho), \\ ESE\left(V_f, E, P1\right) \leq 36J, \end{gathered}$$

where

$$\begin{gathered} 0.3 \leq V_f \leq 0.7, V_{f0} = 0.35, \beta_t = 3, \\ P1 \sim N(1,0.05^2)N, E \sim N(1,0.05^2)GPa, \\ \sum_{e=1}^{nel} \rho_e v_e - V_f \sum_{e=1}^{nel} v_e \leq 0, \\ (0 < \gamma \leq \rho_e \leq 1), \Theta(\rho) = \frac{1}{2}\sigma^T \varepsilon. \end{gathered} \tag{31}$$

Here, ESE (V_f, E, P_1) is the probabilistic performance as constraint computed by volume fraction (V_f) given for the inverse TO-based bisection and two basic variables of E and P_1, which are followed by normal distribution function with mean 1 and standard deviations of 0.05 shown as $P_1 \sim N(1, 0.52)$ or $E \sim N(1, 0.52)$.

The allowable or ultimate constraint is U_c=36J, and the original volume fraction (mean volume fraction) V_{f0} =0.35 in which the objective function for V_{f0} derived for each method is presented in Table 2 in the TO-Normal column.

Table 2. The optimized data derived by STORA for TO and RBTO solutions of different TO methods for MBB beam.

Methods	V_f-(STORA)		V_f-Increment (%)	MPP	TO-Normal		
	TO	RBTO		E	P_1	V_{f0}	Γ
ESO	0.394	0.579	47%	0.9222	1.1282	0.35	41
SIMP	0.476	0.660	39%	0.9222	1.1282	0.35	51.55
MIST	0.450	0.587	31%	0.9222	1.1282	0.35	47.2
Level set	0.4	0.581	46%	0.9222	1.1282	0.35	41

Table 2 depicts the optimal values for TO and RBTO solutions after 7 to 10 iterations. As seen, the MPP values for all the methods are the same. Among all the methods, V_f values for both TO and RBTO are fairly close to each other, though V_f for SIMP is larger than others that are the same as the SIMP for RBTO. Moreover, the value of objective function for the mean V_{f0} of the SIMP method is greater than the others. On the other hand, more maximization has been extracted for the ESO (XFEM-ESO) method followed by the level set method. Figure 14 demonstrates the optimal topologies derived for TO and RBTO solutions employing the STORA approximations. It is highlighted that the design acquired considering uncertainties is significantly different from the deterministic optimization. Each RBTO design ends in a structure with more materials and ribs inside, leading to more safety and reliability. While the most change is achieved in the ESO (XFEM-ESO) method, where larger ribs are added to the structure, in the MIST method, the inner ribs become thicker and supports are vanished.

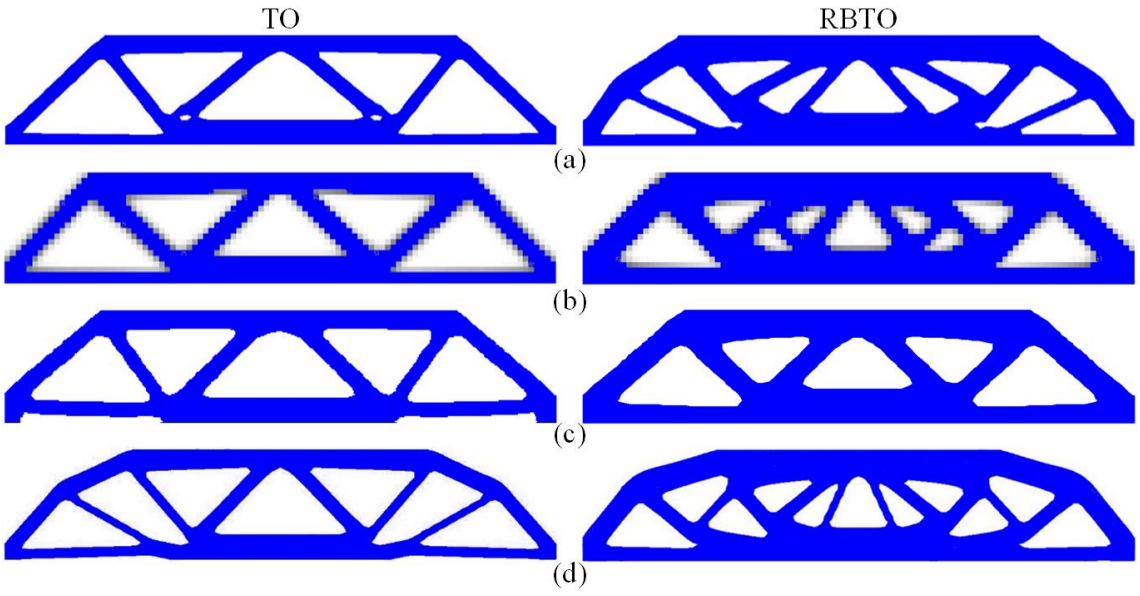

Figure 14. The optimal topologies of TO and RBTO solutions derived by the RBTO approximation for different TO methods for MBB structure a) Level set, b) SIMP, c) MIST, and d) ESO.

Figure 15 compares different TO approaches in inverse TO and RBTO solutions. As can be seen, RBTO solutions comprise a solution for arriving to the U_c at the minimum time with fewer variations.

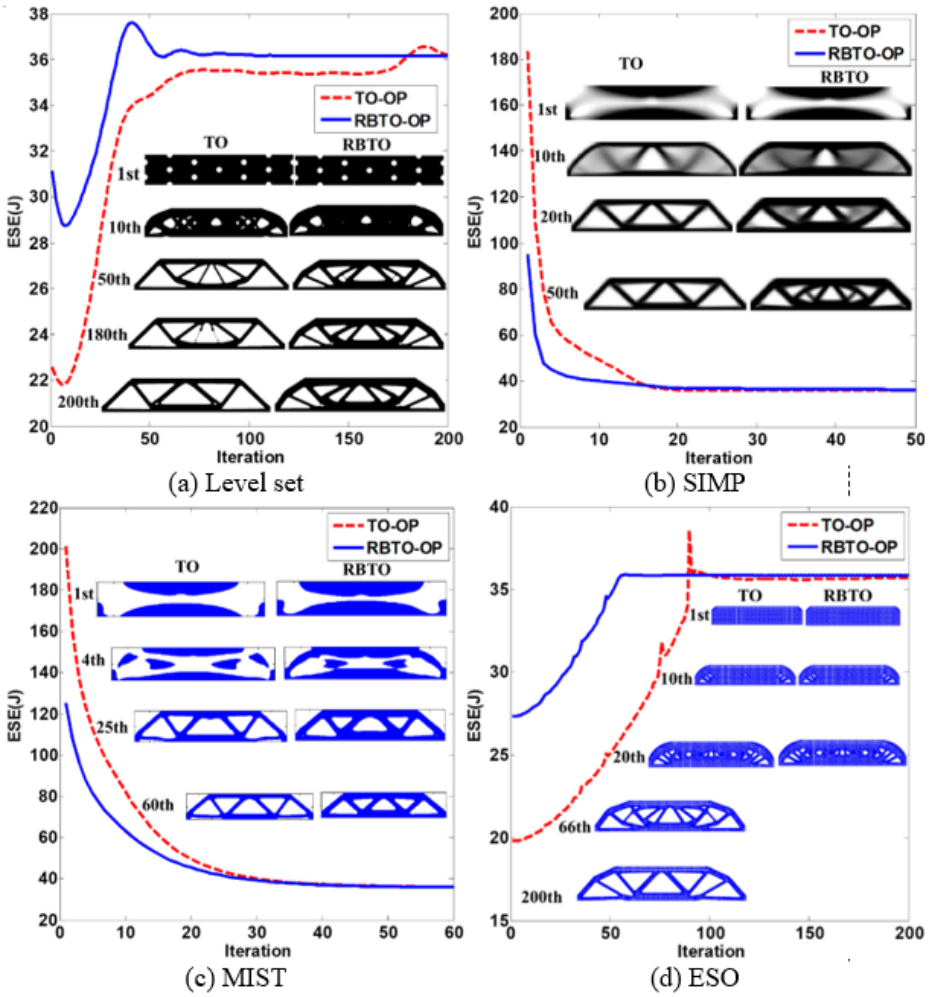

Figure 15. The curves of comparison of TO and RBTO solutions for different TO approaches of the MBB structure. Several snapshots of the design domain throughout the optimization process are presented to illustrate the evolution of the structure.

Figure 16 demonstrates the different layouts of MBB structure for four reliable cases given from different target reliability indices, i.e., β_t = 1, 2, 4, and 5. It can be found that by increasing the reliability index from 1 to 5, the volume fraction increases from 0.4546 to 0.7986, which is related to a nonlinear results based on the reliability index. There is a 10% increase in V_f when β_t changes from 1 to 2, and is about 17% when changing β_t from 4 to 5. Thus, by increasing β_t, the material used is enlarged, which in causes more ribs in the structure. By increasing the safety related to reliability index, load increases and elasticity modulus decline for this structure. Consequently, to receive a structure with a stiffer design, the volume fraction must increase, as presented in Figure 16.

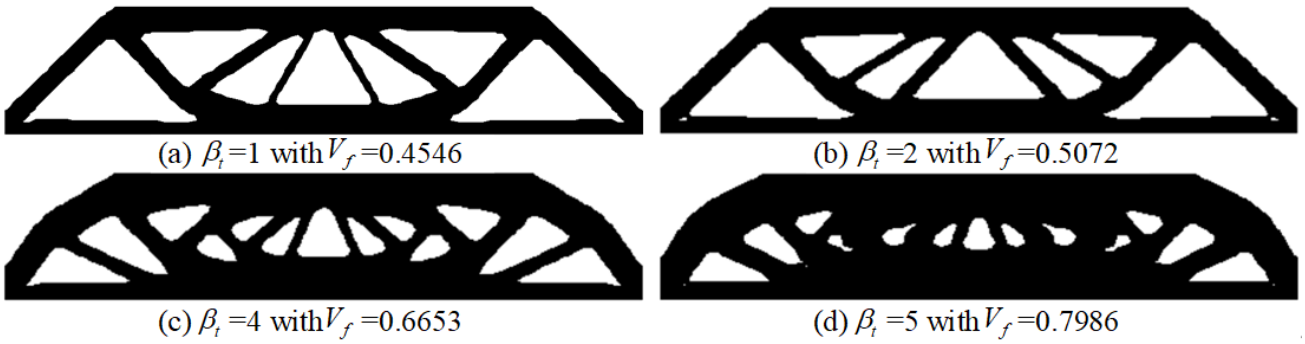

Figure 16. Shape optimum layout obtained by the level set method and DMV for different target reliability indices for MBB structure.

5.2.2. Example 4 L-shape structure

As illustrated in Figure 17, the third example is devoted to the RBTO study of an L-shape structure. This plate structure, with the geometrical dimensions given in Figure 17, is fixed at the top edge. Here, the concentrated force F (or P_1) is imposed on the top corner of the right side of the plate. Assume that the Young's modulus and load are 2 and 0.1, respectively, and the external load and elasticity modulus are normal random variables with COV =0.05 and the total strain energy ESE U_c=0.6J as the maximum allowable constraint. V_f mean (V_{f0}) is 0.25. The plate is discretized into 6400 same-sized elements. The TO problem is solved by three TO procedures, i.e., MIST, ESO (XFEM-ESO), and level set. The specified predefined parameters for each method are given as follows:

I. MIST method: $rmin$=0.03, $penal$=3, dynamic move limit.
II. ESO (XFEM-ESO): the same as Example 2 [73].
III. Level set: same as Example 2.

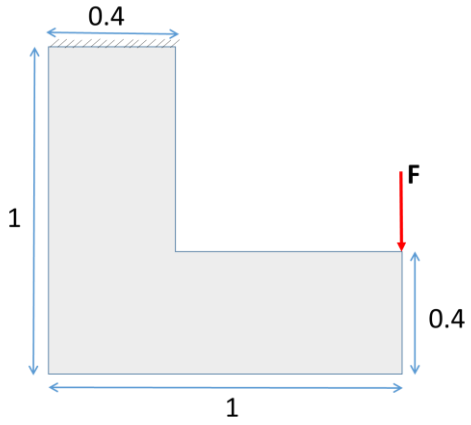

Figure 17. An L-shape structure under a concentrated load fixed at the top edge.

Eq (35) is implemented to solve the RBTO optimization problem in finding optimal V_f for TO and RBTO solutions as follows:

$$\text{Find} \quad V_f,$$

$$\min \quad f(\mathrm{d}) = V_f,$$

$$\text{S.t.} \quad \mathrm{K}(\rho)\mathrm{Y}(\rho) = \mathrm{F}(\rho),$$

$$ESE\left(V_f, E, P1\right) \leq 0.6J,$$

where

$$0.2 \leq V_f \leq 0.7, V_{f0} = 0.25, \beta_t = 3,$$
$$P1 \sim N(0.1, 0.005^2)N, E \sim N(2, 0.1^2)GPa, \tag{32}$$
$$\sum_{e=1}^{nel} \rho_e v_e - V_f \sum_{e=1}^{nel} v_e \leq 0,$$
$$(0 < \gamma \leq \rho_e \leq 1), \Theta(\rho) = \frac{1}{2}\sigma^T \varepsilon.$$

Table 3 and Figure 18 are employed to embody the numerical results. Results were obtained approximately after 11 iterations for each RBTO solution. The TO model using SIMP does not provide a stable optimum shape layout. The level set and the MIST method are more stable than the SIMP for this problem. From the results adopted above, the following points can be extracted:

1) The optimal amount of the relative volume fraction derived by the RBTO model enlarges, i.e., 0.318 to 0.48 for ESO (34%), 0.361 to 0.515 for MIST (30%), and 0.23 to 0.3127 for the level set (26%). That is, a more rigorous necessity of safety inevitably concludes to a lesser cost-effective design.
2) The MPP values are the same for each method. Although V_{f0} and the optimized objective functions Γ and V_f increase, in the case of considering V_{f0}, they are relatively similar for the MIST and ESO (XFEM-ESO); however, they are larger in comparison with the level set. The optimum results as Γ for the level set method is less than other TO methods. The level set method provides the lowest V_f among the others, so the TO methods are significantly affected on the optimum volume fraction, meaning that these optimum results depend on the formulation and searching process of TO methods.
3) Structural features among the deterministic design and the RBTO model may have substantial dissimilarity and differences, which depicts the importance of accounting and considering uncertainties in the topology optimization of continuum solid structures. This is because of creating more ribs inside the structure. Remember that the deterministic approximation needs lower material but leads to a great value of lower reliability, resulting in serious safety jeopardy.
4) Figure 18 shows that the constraints in the TO and RBTO methods are converged to the same values, the optimum of the TO model. Therefore, the bisection coupled with the TO method for finding the optimum V_f is a capable and robust method for application in the inverse TO methods. By comparing TO results with deterministic and random variables, the optimum results of Γ are the same as U_c for all TO models.

Table 3. The optimized values and V_{f0} for different TO methods of an L-shape structure.

Methods	V_f-(STORA)		V_f-Increment (%)	MPP		TO-Normal	
	TO	RBTO		E	P_1	V_{f0}	Γ
ESO	0.318	0.48	34%	1.8443	0.1128	0.25	0.732
MIST	0.361	0.515	30%	1.8443	0.1128	0.25	0.873
Leve set	0.23	0.3127	26%	1.8443	0.1128	0.25	0.53

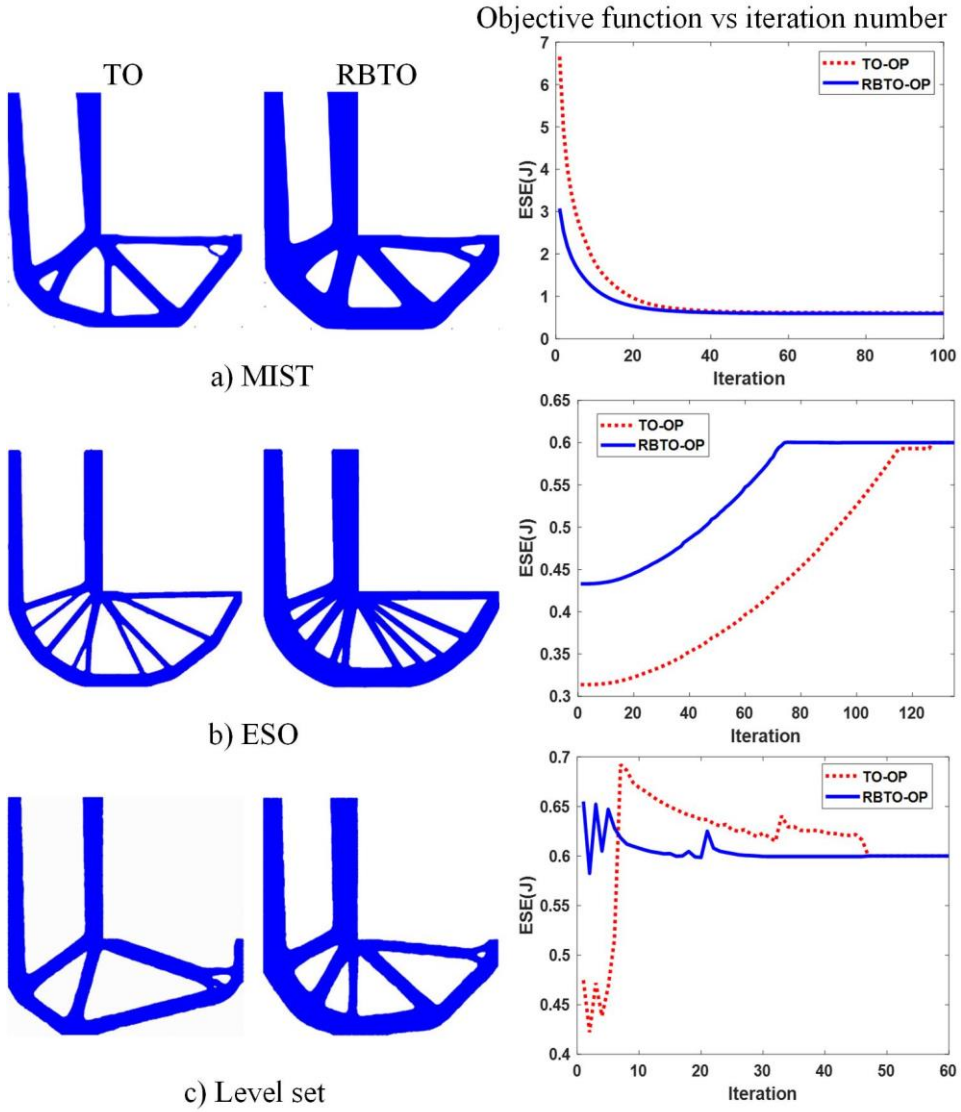

Figure 18. Optimal layouts derived for TO and RBTO solutions of three optimization schemes vs the iteration histories of Γ for different TO methods applied in L-shape problems a) MIST, b) ESO, and c) Level set.

5.2.3. Example 5-Passive elements

In some cases, because of having passive elements in the FEM domain, such as a hole in a plate, those elements must not be involved in the optimal shape, because optimal shape takes the advantage

of the presence of other elements than passive elements to form the final shape. This example investigates TO and RBTO of a plate with $nelx$ =100 elements in x direction and $nely$ =50 elements in y direction with a circle having a center ($nely$/2, $nelx$/3) and radius of $nelx$/3, originally presented in [57]. A point load P_1, as shown in Figure 19, is applied downward at the lower corner of the right edge while the left side is clamped. The aim is to find V_f or X(MPP) and optimal shapes for the TO and RBTO problems by the STORA procedure with the uncertainties of P_1 and elasticity modulus E with the mean values of P_1 and E equal to 1. The Poisson's ratio is υ =0.3. The objective function Γ is the total strain energy of the plate with allowed probabilistic value, U_c=136.5J, and the mean volume fraction, V_{f0}=0.4. The TO and RBTO problems are given in Eq. (36), solved by six TO approaches, i.e., SIMP1(con2D), Level set1(Filterbased), BESO(Multiscale), SIMP2, Level set2, and Tobs101. The results are compared with each other.

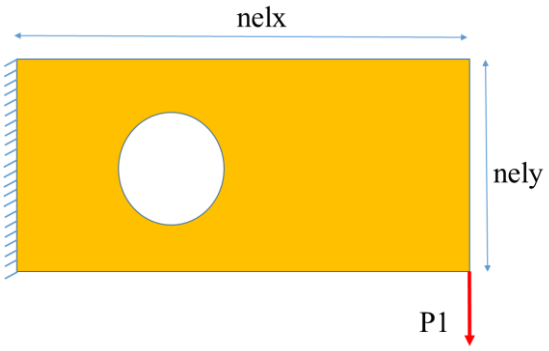

Figure 19. A plate with white region as passive elements in a FEM mesh.

$$\begin{aligned} &\text{Find} \quad V_f, \\ &\min \quad f(\mathrm{d}) = V_f, \\ &\text{S.t.} \quad \mathrm{K}(\rho)\mathrm{Y}(\rho) = \mathrm{F}(\rho), \\ &ESE\left(V_f, E, P\,1\right) \le 136.5J, \end{aligned}$$

where

$$\begin{aligned} &0.2 \le V_f \le 0.7, V_{f0} = 0.4, \beta_t = 3, \\ &P1 \sim \frac{N\left(1,0.05^2\right)N}{m}, E \sim N(1,0.05^2)GPa, \\ &\sum_{e=1}^{nel} \rho_e v_e - V_f \sum_{e=1}^{nel} v_e \le 0, \\ &(0 < \gamma \le \rho_e \le 1), \Theta(\rho) = \frac{1}{2}\sigma^T \varepsilon. \end{aligned} \tag{33}$$

Specified initial parameters for each TO methods are as follow:

I. SIMP1 method: $penal$=3 and $rmin$=2 [66]. BESO method: $penal$=3, $rxmin$ =2, $rymin$ =2, er=0.02 [68]. $rxmin$ and $rymin$ are utilized for the filtering of the sensitivities of the macro-scale and filtering of the sensitivities of the micro-scale, respectively.

II. Tobs101 method: $gbar$ =0.261, $epsilons$ =0.01, $beta$ =0.05, and $rmin$=2 [93]. In the Tobs101 method, $gbar$ is the prescribed constrained values, epsilons define the move limits for the constraint functions, and beta states the truncation error constraint parameter.

III. Other methods are the same as previous examples.

Table 4 illustrates the results of MPP, optimized V_f for TO, RBTO, and mean V_{f0}. It enables comparisons between different TO methods applied to derive the results. It shows that MPP results are the same for all methods and identical to the values in examples 1 and 3. In terms of optimized Γ for V_{f0}=0.4, the largest value is for the SIMP2 method, while the Level set1 (Filter based) method takes the lowest value equal to 84J. Overall, the optimized V_f for the RBTO solution of all methods are the same; however, the value for the SIMP2 is bigger than others, though the largest percentage increase for V_f belongs to the BESO approach. On the other hand, the TO results are approximately close to each other, nearly around 0.25; nevertheless, the Tobs101 assigns the lowest value 0.261 with the lowest percentage of V_f increment, along with the Level set2 followed by SIMP1(con2D) with 0.25 and Level set1 and SIMP2 with 31% increments.

Table 4. The values for MPP, V_f for TO and RBTO, and TO with mean V_{f0} of a plate with passive elements.

Methods	V_f -(STORA)		V_f -Increment (%)	MPP		TO-Normal	
	TO	RBTO		E	P_1	V_{f0}	Γ
SIMP1	0.288	0.383	25	0.9222	1.1282	0.4	94
Level set1	0.2248	0.324	31	0.9222	1.1282	0.4	84
BESO	0.276	0.415	34	0.9222	1.1282	0.4	101
SIMP2	0.3	0.435	31	0.9222	1.1282	0.4	106
Level set2	0.268	0.3688	28	0.9222	1.1282	0.4	93
Tobs101	0.261	0.383	28	0.9222	1.1282	0.4	98

Figure 20 displays the variations in objective functions with the iteration numbers throughout the optimization course for TO and RBTO. As it is depicted, all the optimization processes converge to the U_c for TO and RBTO after many iterations in which the iteration number for RBTO is less than TO.

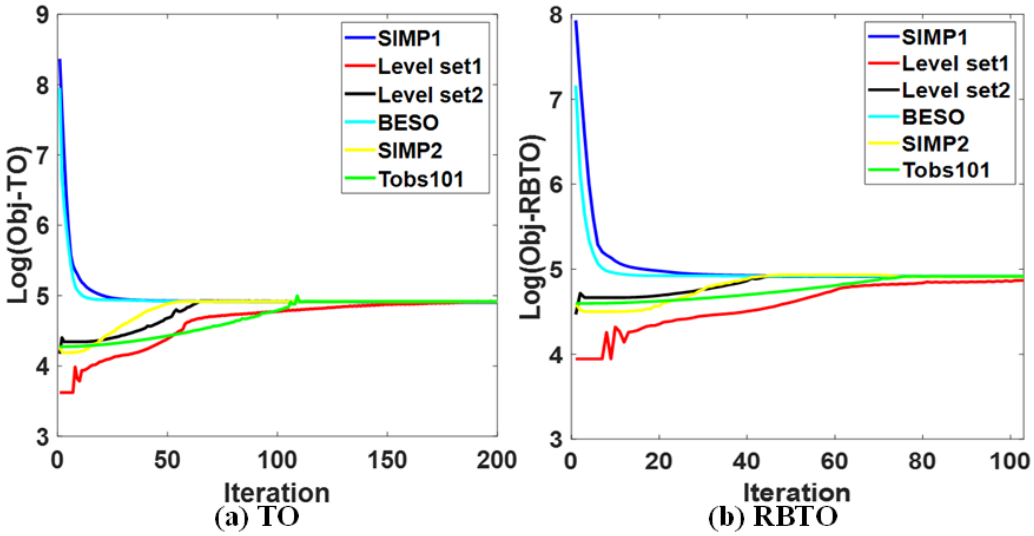

Figure 20. The histories of TO and RBTO within the optimization process as SIMP1, Level set1, Level set2, BESO, SIMP2, and Tobs101in 200 iteration numbers for different TO approaches for Example 5.

The optimal topologies derived by different TO approaches are given in Figure 21 for TO and RBTO solutions using V_f applying MPP values. Comparisons of the results reveal that the optimal solutions obtained by RBTO have distinct topologies from those attained by TO. As can be seen, applying RBTO methodology results in a stronger structure with greater ability against changes in loads due to more internal members. Among them, in BESO (Multiscale) and Tobs101, changes in optimal shapes from TO to RBTO are significant, while in SIMP1 (con2D), fewer variants appear.

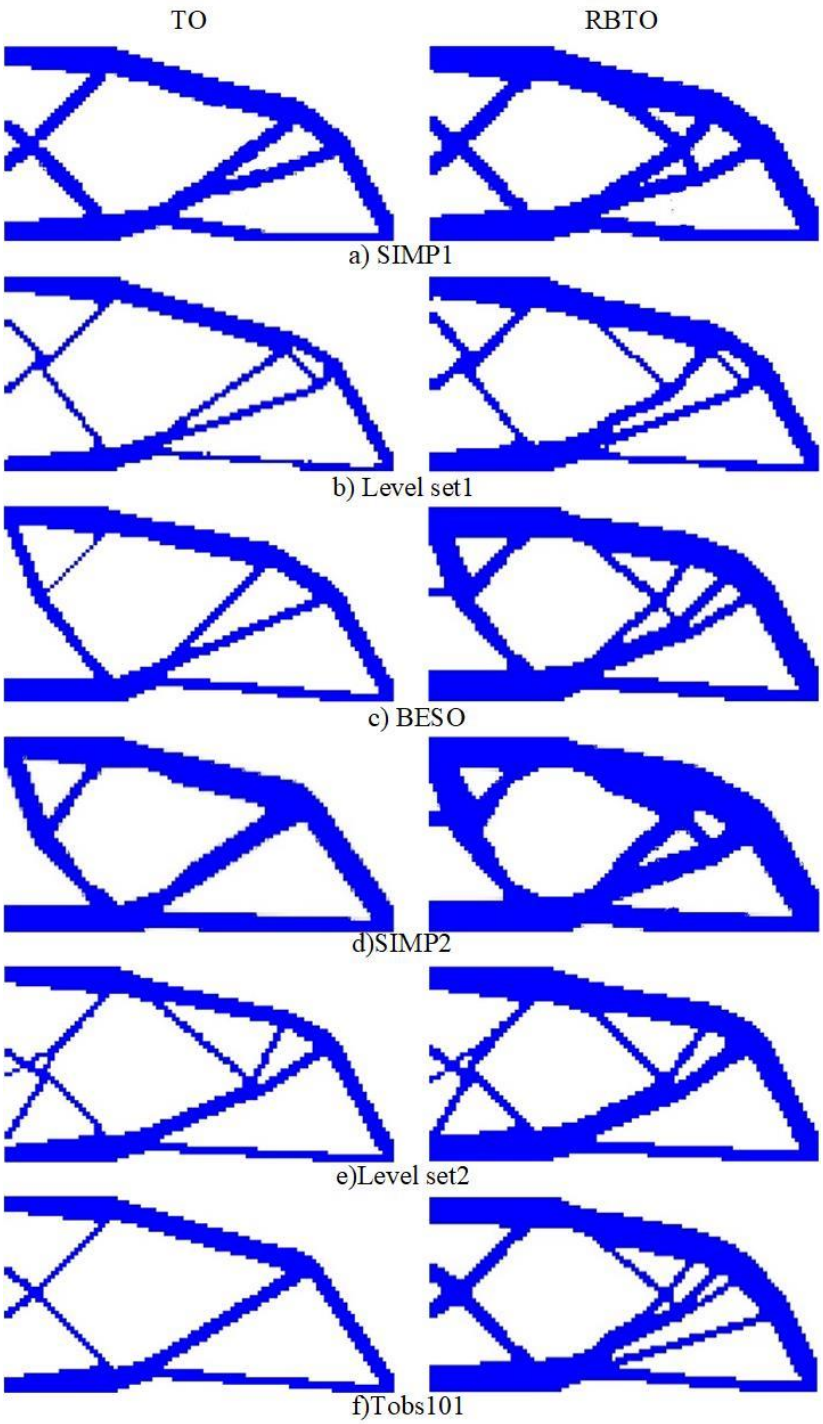

Figure 21. Optimal shapes of a passive structure for different TO approaches, including a) SIMP1, b) Level set1, c) BESO, d) SIMP2, and e) Level set2 in TO and RBTO solutions for Example 5.

5.2.4. Example 6-Tie-arch bridge structure

In this example, we look at the TO and RBTO optimization problem solutions of a Tie-arch bridge structure with the aid of three different TO methods, i.e., SIMP (top88) [64], GPM, and Level set (filter

based). We adopted a Tie-arch bridge as an example originally presented by Feijóo, et al., [94] and then employed by Yaghmaei, et al. [87], where its geometrical dimensions, loading, and boundary conditions are shown in Figure 22. The design field is 180×60 discretized into 270×180 analogous finite elements. $\bar{q}$ is an equivalent traffic loading with the mean value equal to 1. Because of symmetry in the shape of the bridge, only half the bridge is considered for optimization problem resolution. In the optimization process, the aim is to find optimized volume fraction with the mean volume fraction V_{f0}=0.3 and relevant $rmin$, which is given for each optimization method later. Normal random variables, as the constraints, are elasticity modulus and $\bar{q}$. The upper limit of objective function Γ, as the probabilistic constraint, is U_c =85J. Eq. (34) is employed for representing the optimization problem and the TO and RBTO solutions under uncertainties.

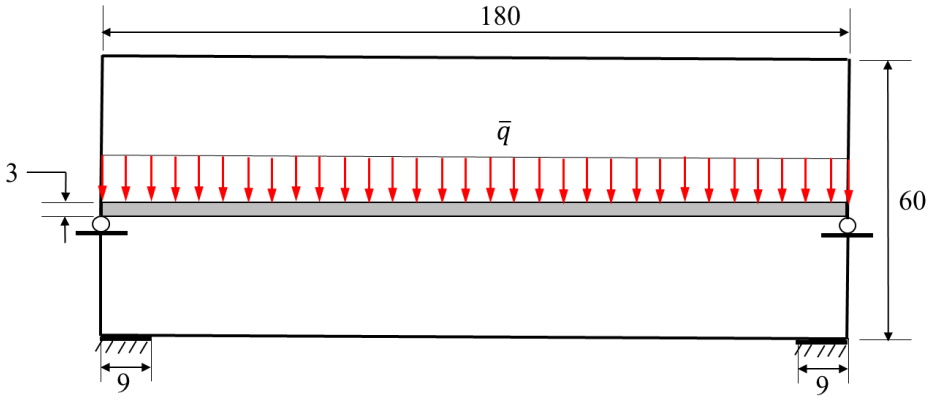

Figure 22. Design domain of a Tie-arch bridge with geometrical dimensions, loading, and supports.

$$\begin{aligned} &\text{Find} \quad V_f, \\ &\min \quad f(\mathrm{d}) = V_f, \\ &\text{S.t.} \quad \mathrm{K}(\rho)\mathrm{Y}(\rho) = \mathrm{F}(\rho), \\ &ESE\left(V_f, E, \bar{q}\right) \le 85J, \end{aligned}$$

where

$$\begin{aligned} &0.2 \le V_f \le 0.7, V_{f0} = 0.3, \beta_t = 3, \\ &\bar{q} \sim \frac{N\left(1,0.05^2\right)N}{m}, E \sim N(1,0.05^2)GPa, \\ &\sum_{e=1}^{nel} \rho_e v_e - V_f \sum_{e=1}^{nel} v_e \le 0, \\ &(0 < \gamma \le \rho_e \le 1), \Theta(\rho) = \frac{1}{2}\sigma^T \varepsilon, \end{aligned} \tag{34}$$

Specified initial parameters for each TO method are as follow:

I. SIMP (top88) method: $penal$ =3, $rmin$=2 and ft =1 [64].

II. GPM method: $loop-limit$ =100, $penal$=3 and $rmin$=1 [65].

III. Level set (FilterBased) method: PI = [10, 8], I_E =0, dt= 0.1, T =6, $Tinf$ =40, $penal$=100, and $rmin$=1 [86]. PI is proportional gain/integral gain, I_E is initial value for integral part, dt is factious time step, T is the time at which volume fraction is expected to reach V_{max}, and $Tinf$ is the total time for an optimization process equal to $Tinf/dt$.

Initially, by the mean value of the volume fraction, the optimized value and elemental information are derived. These elemental details, along with the probabilistic constraint, are used to extract MPP. Next, MPP values are utilized by the bisection method to obtain optimized values of the volume fraction and thereby RBTO shape. In addition, the optimized TO volume fraction and its optimized layout are also derived by the mean values of E and $\bar{q}$.

The STORA procedure is applied for the solution of the optimization problems for each TO method. The results extracted are approximately after 10 iterations and are summarized in Table 5 and Figures 23–25.

Table 5. Results for the TO and RBTO solutions of a Tie-arch bridge structure.

Methods	V_f-(STORA)		V_f-Increment (%)	MPP		TO-Normal	
	TO	RBTO		E	P_1	V_{f0}	Γ
SIMP	0.249	0.342	27.2	0.9222	1.1282	0.3	70
GPM	0.285	0.354	19.5	0.9222	1.1282	0.3	70
Level set	0.2621	0.358	26.78	0.9222	1.1282	0.3	75

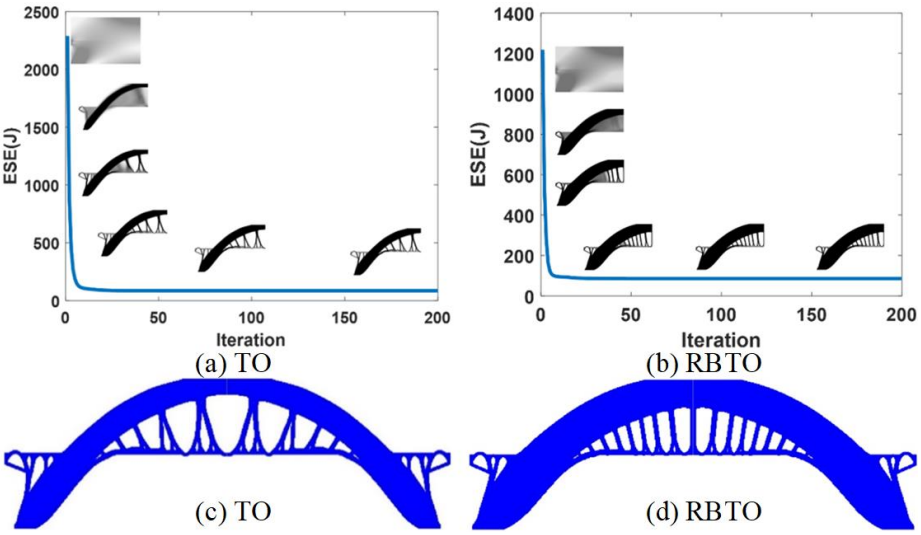

Figure 23. TO and RBTO solutions using SIMP (top88) for optimal designs of a bridge problem a) evolution histories of b) optimal layouts.

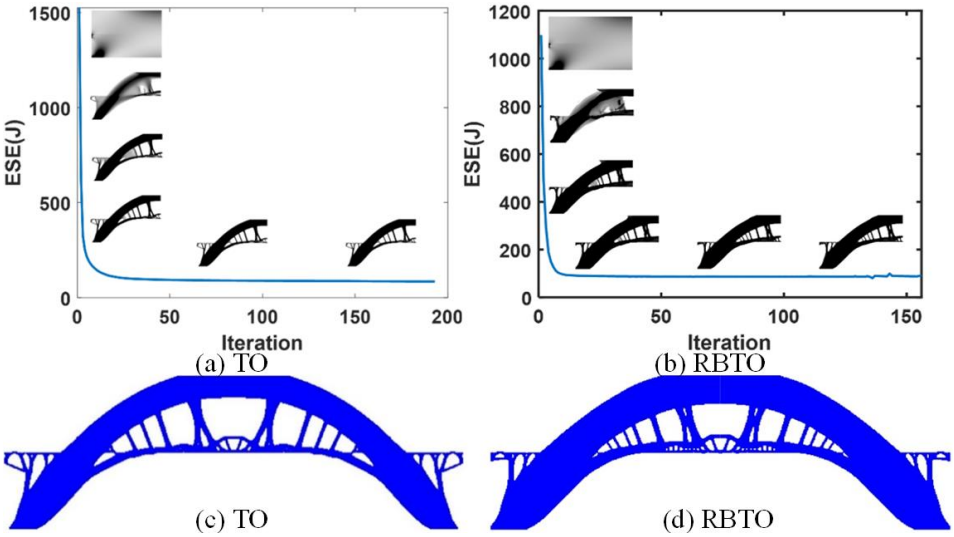

Figure 24. TO and RBTO solutions using GPM for optimal designs of a bridge problem a) evolution histories of b) optimal layouts.

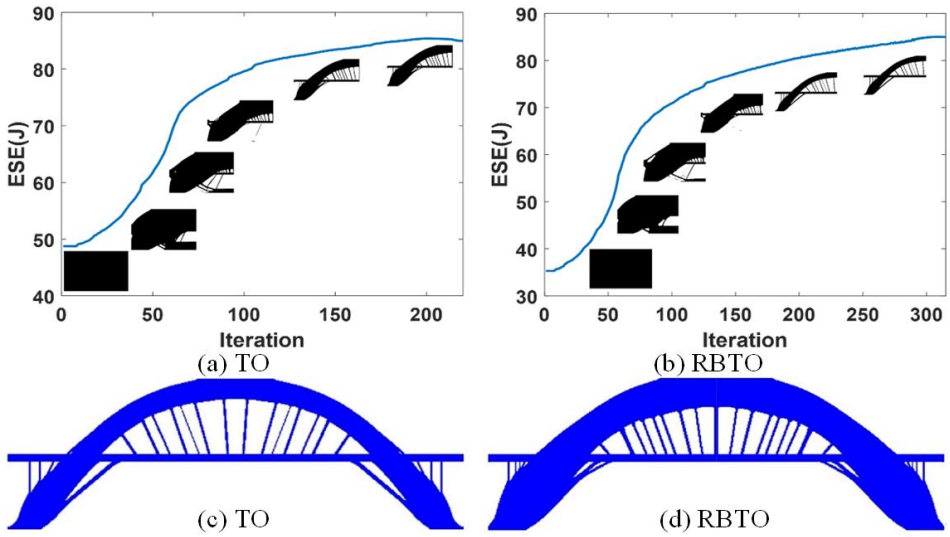

Figure 25. TO and RBTO solutions using Level set (FilterBased) for optimal designs of a bridge problem a) evolution histories of b) optimal layouts.

As can be seen, the MPP values are the same for all methods besides the optimized objective values with mean volume fractions V_{f0} roughly the same. It is seen that the represented RBTO generates superior volume fraction than deterministic topology optimization, which is due to the fact that the considered RBTO consumes excess material to guarantee that the probabilistic constraint is fulfilled in the existence of uncertainties, while the deterministic topology optimization overlooks the uncertainties. This means that reducing lower, allowable failure possibility results in the material volume of the designs produced by the proposed RBTO to be increased in which larger materials are required to strengthen the structural stiffness. Furthermore, lower volume fraction assigned to the TO solution indicates increased violation of the possibility constraint and consequently the unreliability of TO methods. Alternatively, the amount of failure is possibly related to the RBTO solution because it

does not surpass the upper limit of probabilistic constraint, implying that the derived volume fraction by the RBTO solution addresses the allowable failure possibility, strictly.

The increment percentage of volume fraction from TO to RBTO is considerable where SIMP (top88) has the highest percentage.

Figures 23–25 display the iteration history of the optimization process of the proposed TO and RBTO procedures, including some snapshots of design domain evolution to the global convergence of optimization process. As can be observed, the optimization process is stable from the initial values to the upper limit of probability constraint. It is seen that the RBTO solution begins with lower values in the cases of SIMP and GPM and more value in case of the level set method.

Interestingly, the RBTO solution yields an optimized feature that is different from the TO solution with more material and more ribs inside the bridge, reflecting that the optimized structure has more reliability and safety with the TO solution.

Author contributions

The authors confirm contribution to the paper as follows: Conceptualization, Yiqing Shi, Mahmoud Alfouneh and Chao Yuan; methodology, Yiqing Shi, Mahmoud Alfouneh and Chao Yuan; software, Yiqing Shi, Mahmoud Alfouneh and Chao Yuan; validation, Yiqing Shi, Mahmoud Alfouneh and Chao Yuan; formal analysis, Yiqing Shi, Mahmoud Alfouneh and Chao Yuan; investigation, Yiqing Shi, Mahmoud Alfouneh and Chao Yuan; resources, Yiqing Shi; data curation, Yiqing Shi, Mahmoud Alfouneh and Chao Yuan; writing—original draft preparation, Yiqing Shi, Mahmoud Alfouneh and Chao Yuan; writing—review and editing, Yiqing Shi, Mahmoud Alfouneh and Chao Yuan; visualization, Mahmoud Alfouneh and Chao Yuan; supervision, Yiqing Shi, Mahmoud Alfouneh and Chao Yuan; project administration, Yiqing Shi, Mahmoud Alfouneh and Chao Yuan; funding acquisition, Yiqing Shi, Mahmoud Alfouneh and Chao Yuan. All authors reviewed the results and approved the final version of the manuscript.

Use of Generative-AI tools declaration

The author declares she has not used Artificial Intelligence (AI) tools in the creation of this article.

Acknowledgments

This research was funded by the National Key Research and Development Program (Grant No. 2022YFB3706904).

Conflict of interest

The authors declare no conflicts of interest.

References

1. M. Bendsøe, N. Kikuchi, Generating optimal topologies in structural design using a homogenization method, *Comput. Method. Appl. M.*, **71** (1988), 197–224. https://doi.org/10.1016/0045-7825(88)90086-2
2. M. Habashneh, M. Movahedi Rad, Reliability based geometrically nonlinear bi-directional evolutionary structural optimization of elasto-plastic material, *Sci. Rep.*, **12** (2022), 5989. https://doi.org/10.1038/s41598-022-09612-z
3. M. Bayat, O. Zinovieva, F. Ferrari, C. Ayas, M. Langelaar, J. Spangenberg, et al., Holistic computational design within additive manufacturing through topology optimization combined with multiphysics multi-scale materials and process modelling, *Prog. Mater. Sci.*, **138** (2023) 101129. https://doi.org/10.1016/j.pmatsci.2023.101129
4. B. Wang, Q. Zhu, S. Li, Stabilization of discrete-time hidden semi-Markov jump linear systems with partly unknown emission probability matrix, *IEEE T. Automat. Contr.*, **69** (2023), 1952–1959. https://doi.org/10.1109/TAC.2023.3272190
5. D. Meng, H. Yang, S. Yang, Y. Zhang, A. M. P. De Jesus, J. Correia, et al., Kriging-assisted hybrid reliability design and optimization of offshore wind turbine support structure based on a portfolio allocation strategy, *Ocean Eng.*, **295** (2024), 116842. https://doi.org/10.1016/j.oceaneng.2024.116842
6. Q. Zhu, H. Wang, Output feedback stabilization of stochastic feedforward systems with unknown control coefficients and unknown output function, *Automatica*, **87** (2018), 166–175. https://doi.org/10.1016/j.automatica.2017.10.004
7. M. Habashneh, M. Movahedi Rad, Plastic-limit probabilistic structural topology optimization of steel beams, *Appl. Math. Model.*, **128** (2024) 347–369. https://doi.org/10.1016/j.apm.2024.01.029
8. B. dos Santos, C. da Silva, W. Machado, Uncertainty quantification of the stochastic process "crack size" for the Forman model using the "fast crack bounds" method, *Appl. Math. Model.*, **119** (2023), 500–512. https://doi.org/10.1016/j.apm.2023.03.008
9. Z. Kang, Y. Luo, Non-probabilistic reliability-based topology optimization of geometrically nonlinear structures using convex models, *Comput. Method. Appl. M.*, **198** (2009), 3228–3238. https://doi.org/10.1016/j.cma.2009.06.001
10. L. Wang, B. Ni, X. Wang, Z. Li, Reliability-based topology optimization for heterogeneous composite structures under interval and convex mixed uncertainties, *Appl. Math. Model.*, **99** (2021), 628–652. https://doi.org/10.1016/j.apm.2021.06.014
11. H. Xia, Z. Qiu, An efficient sequential strategy for non-probabilistic reliability-based topology optimization (NRBTO) of continuum structures with stress constraints, *Appl. Math. Model.*, **110** (2022), 723–747. https://doi.org/10.1016/j.apm.2022.06.021
12. X. Zhang, G. Ouyang, A level set method for reliability-based topology optimization of compliant mechanisms, *Sci. China E-Technol. Sci.*, **51** (2008) 443–455. https://doi.org/10.1007/s11431-008-0039-3
13. Z. Li, L. Wang, G. Xinyu, A level set reliability-based topology optimization (LS-RBTO) method considering sensitivity mapping and multi-source interval uncertainties, *Comput. Method. Appl. M.*, **419** (2024), 116587. https://doi.org/10.1016/j.cma.2023.116587

14. Z. Lei, J. Zhang, Y. Liang, G. Chen, D. Yang, Efficient two-phase approach to reliability-based discrete variable topology optimization of continuum structures with multimodal distributions, *Comput. Method. Appl. M.*, **415** (2023), 116237. https://doi.org/10.1016/j.cma.2023.116237
15. Y. Zheng, D. Da, H. Li, M. Xiao, L. Gao, Robust topology optimization for multi-material structures under interval uncertainty, *Appl. Math. Model.*, **78** (2020), 627–647. https://doi.org/10.1016/j.apm.2019.10.019
16. H. Simonetti, V. Almeida, F. de Assis das Neves, V. Del Duca Almeida, L. de Oliveira Neto, Reliability-based topology optimization: an extension of the SESO and SERA methods for three-dimensional structures, *Appl. Sci.*, **12** (2022), 4220. https://doi.org/10.3390/app12094220
17. G. Zhang, C. Liang, Q. Zhu, Adaptive fuzzy event-triggered optimized consensus control for delayed unknown stochastic nonlinear multi-agent systems using simplified ADP, *IEEE T. Automat. Sci. Eng.*, **22** (2025), 11780–11793. https://doi.org/10.1109/TASE.2025.3540468
18. B. Keshtegar, M. Alfouneh, SVR-TO-APMA: Hybrid efficient modelling and topology framework for stable topology optimization with accelerated performance measure approach, *Comput. Method. Appl. M.*, **404** (2023), 115762. https://doi.org/10.1016/j.cma.2022.115762
19. R. Rubinstein, D. Kroese, *Simulation and the Monte Carlo method*, John Wiley & Sons, 2016. https://doi.org/10.1002/9781118631980
20. B. Wang, Q. Zhu, S. Li, Stability analysis of discrete-time semi-Markov jump linear systems with time delay, *IEEE T. Automat. Contr.*, **68** (2023), 6758–6765. https://doi.org/10.1109/TAC.2023.3240926
21. C. Sundararajan, *Probabilistic structural mechanics handbook: Theory and industrial applications*, Springer Science & Business Media, 2012.
22. R. Lopez, A. Beck, Reliability-based design optimization strategies based on FORM: a review, *J. Braz. Soc. Mech. Sci. Eng.*, **34** (2012), 506–514. https://doi.org/10.1590/S1678-58782012000400012
23. Z. Hu, R. Mansour, M. Olsson, X. Du, Second-order reliability methods: a review and comparative study, *Struct. Multidisc. Optim.*, **64** (2021), 3233–3263. https://doi.org/10.1007/s00158-021-03013-y
24. Z. Meng, H. Zhou, H. Hu, B. Keshtegar, Enhanced sequential approximate programming using second order reliability method for accurate and efficient structural reliability-based design optimization, *Appl. Math. Model.*, **62** (2018), 562–579. https://doi.org/10.1016/j.apm.2018.06.018
25. D. Meng, S. Yang, A. de Jesus, S. Zhu, A novel Kriging-model-assisted reliability-based multidisciplinary design optimization strategy and its application in the offshore wind turbine tower, *Renew. Energ.*, **203** (2023), 407–420. https://doi.org/10.1016/j.renene.2022.12.062
26. B. Keshtegar, Enriched FR conjugate search directions for robust and efficient structural reliability analysis, *Eng. Comput.*, **34** (2018), 117–128. https://doi.org/10.1007/s00366-017-0524-z
27. S. Yang, D. Meng, H. Wang, C. Yang, A novel learning function for adaptive surrogate-model-based reliability evaluation, *Philos. Trans. R. Soc. A*, **382** (2024), 2264. https://doi.org/10.1098/rsta.2022.0395
28. B. Keshtegar, P. Hao, A hybrid loop approach using the sufficient descent condition for accurate, robust, and efficient reliability-based design optimization, *J. Mech. Des.*, **138** (2016), 121401. https://doi.org/10.1115/1.4034173

29. Y. Luo, M. Zhou, M. Wang, Z. Deng, Reliability based topology optimization for continuum structures with local failure constraints, *Comput. Struct.*, **143** (2014), 73–84. https://doi.org/10.1016/j.compstruc.2014.07.009
30. J. Zhang, M. Xiao, P. Li, L. Gao, Quantile-based topology optimization under uncertainty using Kriging metamodel, *Comput. Method. Appl. M.*, **393** (2022), 114690. https://doi.org/10.1016/j.cma.2022.114690
31. J. Tang, X. Li, C. Fu, H. Liu, L. Cao, C. Mi, et al., A possibility-based solution framework for interval uncertainty-based design optimization, *Appl. Math. Model.*, **125** (2024), 649–667. https://doi.org/10.1016/j.apm.2023.09.010
32. K. Cho, J. Park, M. Im, S. Han, Reliability-based topology optimization of electro-thermal-compliant mechanisms with a new material mixing method, *Int. J. Precis. Eng. Manuf.*, **13** (2012), 693–699. https://doi.org/10.1007/s12541-012-0090-7
33. C. Kim, S. Wang, K. Rae, H. Moon, K. Choi, Reliability-based topology optimization with uncertainties, *J. Mech. Sci. Technol.*, **20** (2006), 494–504. https://doi.org/10.1007/BF02916480
34. B. Youn, K. Choi, Selecting probabilistic approaches for reliability-based design optimization, *AIAA J.*, **42** (2004) 124–131. https://doi.org/10.2514/1.9036
35. A. Torii, R. Lopez, A. Beck, L. Miguel, A performance measure approach for risk optimization, *Struct. Multidisc. Optim.*, **60** (2019), 927–947. https://doi.org/10.1007/s00158-019-02243-5
36. Z. Meng, B. Keshtegar, Adaptive conjugate single-loop method for efficient reliability-based design and topology optimization, *Comput. Method. Appl. M.*, **344** (2019), 95–119. https://doi.org/10.1016/j.cma.2018.10.009
37. J. Zheng, L. Yuan, C. Jiang, Z. Zhang, An efficient decoupled reliability-based topology optimization method based on a performance shift strategy, *J. Mech. Des.*, **145** (2023), 061705. https://doi.org/10.1115/1.4056999
38. D. Meng, S. Yang, A. De Jesus, T. Fazeres-Ferradosa, S. Zhu, A novel hybrid adaptive Kriging and water cycle algorithm for reliability-based design and optimization strategy: Application in offshore wind turbine monopile, *Comput. Method. Appl. M.*, **412** (2023), 116083. https://doi.org/10.1016/j.cma.2023.116083
39. L. Wang, Y. Liu, D. Liu, Z. Wu, A novel dynamic reliability-based topology optimization (DRBTO) framework for continuum structures via interval-process collocation and the first-passage theories, *Comput. Method. Appl. M.*, **386** (2021), 114107. https://doi.org/10.1016/j.cma.2021.114107
40. L. Wang, Z. Li, B. Ni, K. Gu, Non-probabilistic reliability-based topology optimization (NRBTO) scheme for continuum structures based on the parameterized level-set method and interval mathematics, *Comput. Method. Appl. M.*, **373** (2021), 113477. https://doi.org/10.1016/j.cma.2020.113477
41. D. Meng, S. Yang, H. Yang, A. De Jesus, J. Correia, S. Zhu, Intelligent-inspired framework for fatigue reliability evaluation of offshore wind turbine support structures under hybrid uncertainty, *Ocean Eng.*, **307** (2024), 118213. https://doi.org/10.1016/j.oceaneng.2024.118213
42. T. Cho, B. Lee, Reliability-based design optimization using convex linearization and sequential optimization and reliability assessment method, *Struct. Saf.*, **33** (2011), 42–50. https://doi.org/10.1016/j.strusafe.2010.05.003
43. B. Keshtegar, S. Chakraborty, An efficient-robust structural reliability method by adaptive finite-step length based on Armijo line search, *Reliab. Eng. Syst. Safe.*, **172** (2018), 195–206. https://doi.org/10.1016/j.ress.2017.12.014

44. S. Yang, D. Meng, Y. Guo, P. Nie, A. M. P. de Jesus, A reliability-based design and optimization strategy using a novel MPP searching method for maritime engineering structures, *Int. J. Struct. Integr.*, **14** (2023), 809–826. https://doi.org/10.1108/IJSI-06-2023-0049
45. Y. Zhao, Q. Zhu, Stability of highly nonlinear neutral stochastic delay systems with non-random switching signals, *Syst. Control Lett.*, **165** (2022), 105261. https://doi.org/10.1016/j.sysconle.2022.105261
46. B. Keshtegar, Stability iterative method for structural reliability analysis using a chaotic conjugate map, *Nonlinear Dyn.*, **84** (2016), 2161–2174. https://doi.org/10.1007/s11071-016-2636-1
47. D. Meng, S. Yang, Y. Zhang, S. Zhu, Structural reliability analysis and uncertainties-based collaborative design and optimization of turbine blades using surrogate model, *Fatigue Fract. Eng. M.*, **42** (2019), 1219–1227. https://doi.org/10.1111/ffe.12906
48. S. Zhu, B. Keshtegar, N. Trung, Z. M. Yaseen, D. T. Bui, Reliability-based structural design optimization: hybridized conjugate mean value approach, *Eng. Comput.*, **37** (2021), 381–394. https://doi.org/10.1007/s00366-019-00829-7
49. Y. Huang, Y. Lv, Q. Zhu, Stabilization of hybrid stochastic neutral-type systems with non-differentiable delays under high nonlinearity via discrete-time feedback control, *Appl. Math. Comput.*, **495** (2025), 129333. https://doi.org/10.1016/j.amc.2025.129333
50. Q. Zhu, Event-triggered sampling problem for exponential stability of stochastic nonlinear delay systems driven by Le´vy processes, *IEEE T. Automat. Contr.*, **70** (2024), 1176–1183. https://doi.org/10.1109/TAC.2024.3448128
51. B. Keshtegar, S. Chakraborty, Dynamical accelerated performance measure approach for efficient reliability-based design optimization with highly nonlinear probabilistic constraints, *Reliab. Eng. Syst. Safe.*, **178** (2018), 69–83. https://doi.org/10.1016/j.ress.2018.05.015
52. F. Kong, H. Ni, Q. Zhu, C. Hu, T. Huang, Fixed-time and predefined-time synchronization of discontinuous neutral-type competitive networks via non-chattering adaptive control strategy, *IEEE T. Netw. Sci. Eng.*, **10** (2023), 3644–3657. https://doi.org/10.1109/TNSE.2023.3271109
53. M. Alfouneh, B. Keshtegar, STO-DAMV: Sequential topology optimization and dynamical accelerated mean value for reliability-based topology optimization of continuous structures, *Comput. Method. Appl. M.*, **417** (2023), 116429. https://doi.org/10.1016/j.cma.2023.116429
54. L. Mabood, N. Badshah, H. Ali, M. Zakarya, A. Ahmed, A. A. Khan, et al., Multi-scale-average-filter-assisted level set segmentation model with local region restoration achievements, *Sci. Rep.*, **12** (2022), 15949. https://doi.org/10.1038/s41598-022-19893-z
55. L. Mei, Q. Wang, Structural optimization in civil engineering: a literature review, *Buildings*, **11** (2021), 66. https://doi.org/10.3390/buildings11020066
56. Z. Zhu, Q. Zhu, Adaptive event-triggered fuzzy control for stochastic highly nonlinear systems with time delay and nontriangular structure interconnections, *IEEE T. Fuzzy Syst.*, **32** (2023), 27–37. https://doi.org/10.1109/TFUZZ.2023.3287869
57. Z. Houta, T. Huguet, N. Lebbe, F. Messine, Solid isotropic material with penalization-based topology optimization of three-dimensional magnetic circuits with mechanical constraints, *Mathematics*, **12** (2024), 1147. https://doi.org/10.3390/math12081147
58. O. Sigmund, A 99 line topology optimization code written in Matlab, *Struct. Multidisc. Optim.*, **21** (2001), 120–127. https://doi.org/10.1007/s001580050176
59. K. Liu, A. Tovar, An efficient 3D topology optimization code written in Matlab, *Struct. Multidisc. Optim.*, **50** (2014), 1175–1196. https://doi.org/10.1007/s00158-014-1107-x

60. S. Rojas-Labanda, M. Stolpe, An efficient second-order SQP method for structural topology optimization, *Struct. Multidisc. Optim.*, **53** (2016), 1315–1333. https://doi.org/10.1007/s00158-015-1381-2
61. W. Liao, Q. Zhang, H. Meng, An SQP algorithm for structural topology optimization based on majorization-minimization method, *Appl. Sci.*, **12** (2022), 6304. https://doi.org/10.3390/app12136304
62. M. Fanni, M. Shabara, M. Alkalla, A comparison between different topology optimization methods, *MEJ Mansoura Eng. J.*, **38** (2020), 13–24. https://doi.org/10.21608/bfemu.2020.103788
63. T. Zuo, C. Wang, H. Han, Q. Wang, Z. Liu, Explicit 2D topological control using SIMP and MMA in structural topology optimization, *Struct. Multidisc. Optim.*, **65** (2022), 293. https://doi.org/10.1007/s00158-022-03405-8
64. E. Andreassen, A. Clausen, M. Schevenels, B. S. Lazarov, O. Sigmund, Efficient topology optimization in MATLAB using 88 lines of code, *Struct. Multidisc. Optim.*, **43** (2011), 1–16. https://doi.org/10.1007/s00158-010-0594-7
65. Z. Zeng, F. Ma, An efficient gradient projection method for structural topology optimization, *Adv. Eng. Softw.*, **149** (2020), 102863. https://doi.org/10.1016/j.advengsoft.2020.102863
66. J. Gao, Z. Luo, L. Xia, L. Gao, Concurrent topology optimization of multiscale composite structures in Matlab, *Struct. Multidisc. Optim.*, **60** (2019), 2621–2651. https://doi.org/10.1007/s00158-019-02323-6
67. M. Rad, M. Habashneh, J. Lógó, Reliability based bi-directional evolutionary topology optimization of geometric and material nonlinear analysis with imperfections, *Comput. Struct.*, **287** (2023), 107120. https://doi.org/10.1016/j.compstruc.2023.107120
68. Z. Zhu, Q. Zhu, Adaptive neural prescribed performance control for non-triangular structural stochastic highly nonlinear systems under hybrid attacks, *IEEE T. Automat. Sci. Eng.*, **22** (2024), 6543–6553. https://doi.org/10.1109/TASE.2024.3447045
69. X. Huang, M. Xie, *Evolutionary topology optimization of continuum structures: methods and applications*, John Wiley & Sons, 2010. https://doi.org/10.1002/9780470689486
70. X. Huang, Y. Xie, A further review of ESO type methods for topology optimization, *Struct. Multidisc. Optim.*, **41** (2010), 671–683. https://doi.org/10.1007/s00158-009-0447-4
71. G. Rozvany, O. Querin, Combining ESO with rigorous optimality criteria, *Int. J. Veh. Des.*, **28** (2002), 294–299. https://doi.org/10.1504/IJVD.2002.001991
72. Y. Liu, F. Jin, Q. Li, S. Zhou, A fixed-grid bidirectional evolutionary structural optimization method and its applications in tunnelling engineering, *Int. J. Numer. Method. Eng.*, **73** (2008), 1788–1810. https://doi.org/10.1002/nme.2145
73. M. Abdi, Evolutionary topology optimization of continuum structures using X-FEM and isovalues of structural performance, University of Nottingham, 2015.
74. Z. Zhuang, Y. Xie, Q. Li, S. Zhou, A 172-line Matlab code for structural topology optimization in the body-fitted mesh, *Struct. Multidisc. Optim.*, **66** (2023), 11. https://doi.org/10.1007/s00158-022-03464-x
75. G. Kazakis, N. Lagaros, Multi-scale concurrent topology optimization based on BESO, implemented in MATLAB, *Appl. Sci.*, **13** (2023), 10545. https://doi.org/10.3390/app131810545
76. L. Tong, J. Lin, Structural topology optimization with implicit design variable-optimality and algorithm, *Finite Elem. Anal. Des.*, **47** (2011), 922–932. https://doi.org/10.1016/j.finel.2011.03.004

77. M. Alfouneh, V. Hoang, Z. Luo, Q. Luo, Topology optimization for multi-layer multi-material composite structures, *Eng. Optim.*, **55** (2023), 773–790. https://doi.org/10.1080/0305215X.2022.2034801
78. W. Chen, X. Su, S. Liu, Algorithms of isogeometric analysis for MIST-based structural topology optimization in MATLAB, *Struct. Multidisc. Optim.*, **67** (2024), 43. https://doi.org/10.1007/s00158-024-03764-4
79. M. Alfouneh, V. Hoang, Heat flux topology optimization treatment of vibrational damped cellular composite flexible structures, *Optim. Eng.*, **24** (2023), 1747–1772. https://doi.org/10.1007/s11081-022-09751-2
80. W. Chen, L. Tong, S. Liu, Concurrent topology design of structure and material using a two-scale topology optimization, *Comput. Struct.*, **178** (2017), 119–128. https://doi.org/10.1016/j.compstruc.2016.10.013
81. J. Sethian, A. Wiegmann, Structural boundary design via level set and immersed interface methods, *J. Comput. Phys.*, **163** (2000), 489–528. https://doi.org/10.1006/jcph.2000.6581
82. G. Gordon, R. Tibshirani, Karush-kuhn-tucker conditions, *Optimization*, **10** (2012), 725.
83. E. Madenci, I. Guven, *The finite element method and applications in engineering using ANSYS®*, Springer, 2015. https://doi.org/10.1007/978-1-4899-7550-8
84. X. Liu, F. Gasco, W. Yu, J. Goodsell, K. Rouf, Multiscale analysis of woven composite structures in MSC. Nastran, *Adv. Eng. Softw.*, **135** (2019), 102677. https://doi.org/10.1016/j.advengsoft.2019.04.008
85. P. Wei, Z. Li, X. Li, M.Y. Wang, An 88-line MATLAB code for the parameterized level set method based topology optimization using radial basis functions, *Struct. Multidisc. Optim.*, **58** (2018), 831–849. https://doi.org/10.1007/s00158-018-1904-8
86. S. Zhang, P. Li, Y. Zhong, J. Xiang, Structural topology optimization based on the level set method using COMSOL, *CMES Comput. Model. Eng. Sci.*, **101** (2014), 17–31.
87. M. Yaghmaei, A. Ghoddosian, M. M. Khatibi, A filter-based level set topology optimization method using a 62-line MATLAB code, *Struct. Multidisc. Optim.*, **62** (2020), 1001–1018. https://doi.org/10.1007/s00158-020-02540-4.
88. Z. Houta, T. Huguet, N. Lebbe, F. Messine, Solid isotropic material with penalization-based topology optimization of three-dimensional magnetic circuits with mechanical constraints, *Mathematics*, **12** (2024), 1147. https://doi.org/10.3390/math12081147
89. E. Demirci, A. R. Yıldız, A new hybrid approach for reliability-based design optimization of structural components, *Mater. Test.*, **61** (2019), 111–119. https://doi.org/10.3139/120.111291.
90. B. Keshtegar, P. Hao, A hybrid self-adjusted mean value method for reliability-based design optimization using sufficient descent condition, *Appl. Math. Model.*, **41** (2017), 257–270. https://doi.org/10.1016/j.apm.2016.08.031
91. Z. Meng, Y. Pang, Y. Pu, X. Wang, New hybrid reliability-based topology optimization method combining fuzzy and probabilistic models for handling epistemic and aleatory uncertainties, *Comput. Method. Appl. M.*, **363** (2020), 112886. https://doi.org/10.1016/j.cma.2020.112886
92. M. Alfouneh, J. Ji, Q. Luo, Damping design of harmonically excited flexible structures with graded materials to minimize sound pressure and radiation, *Eng. Optim.*, **53** (2021), 348–367. https://doi.org/10.1080/0305215X.2020.1735381

93. R. Picelli, R. Sivapuram, Y. M. Xie, A 101-line MATLAB code for topology optimization using binary variables and integer programming, *Struct. Multidisc. Optim.*, **63** (2021), 935–954. https://doi.org/10.1007/s00158-020-02719-9
94. R. A. Feijóo, A. A. Novotny, C. Padra, E. Taroco, The topological-shape sensitivity method and its application in 2D elasticity, *J. Comput. Method. Sci. Eng.*, **4** (2004), 397–428.

AIMS Press